Date of Publication: 5th February 2026
ISSN: 2737-713X

PROVENANCE OF THE UPPER ORDOVICIAN AJUA SHALE AND ELMINA SANDSTONE FORMATIONS, SEKONDIAN GROUP – GHANA

Dora M. Fianyo, Marian S. Sapah*, Ben Fiebor, Patrick A. Sakyi, and Daniel K. Asiedu

Department of Earth Science, University of Ghana, Legon-Accra, Ghana
***Corresponding author:** msapah@ug.edu.gh

Abstract

The mineralogical and geochemical characteristics of siliciclastic sedimentary rocks are key indicators of their provenance and depositional settings. Despite previous studies on the Sekondian Group in Ghana, a detailed petrographic investigation into the Ajua Shale and Elmina Sandstone Formations has remained limited. This study addresses this gap by integrating petrographic, mineralogical, and geochemical analyses to infer their provenance, weathering history, and tectonic setting. A total of 47 thin sections (20 sandstones from each Formation and 7 sandy shale samples from the Ajua Shale Formation) were analyzed petrographically using point-counting methods under a polarizing microscope. X-ray diffraction (XRD) was conducted on ten samples for mineralogical characterization. Additionally, 40 powdered samples underwent major and trace element geochemical analysis using X-ray fluorescence (XRF). Data were interpreted using standard ternary diagrams, weathering indices (Chemical Index of Alteration (CIA), Chemical Index of Weathering (CIW), Plagioclase Index of Alteration (PIA), Index of Compositional Variability (ICV), and tectonic discrimination plots. Petrographic analysis classifies the sandstones predominantly as arkosic and sub-arkosic arenites, characterized by sub-mature textures and low chemical maturity, with high feldspar and quartz content. Geochemically, both formations exhibit weak to moderate chemical weathering, reflected in the CIA and PIA values. The Al_2O_3/TiO_2 and TiO_2/Zr ratios, along with enrichments in Zr, Hf, and Y, suggest felsic to intermediate igneous sources, likely the Birimian granitoids and Pan-African felsic gneisses. Tectonic discrimination diagrams position the sandstones mainly in dissected arc and active continental margin fields, although field evidences also hint at passive margin conditions due to low sedimentation rates and the absence of volcanism. The integrated petrographic and geochemical data indicate that the Ajua Shale and Elmina Sandstone Formations were derived from felsic-intermediate continental sources, deposited under semi-arid to arid climates, and influenced by active margin tectonics, with possible overprinting from glacial and passive margin settings during the Late Ordovician.

Keywords
Upper Ordovician, Sekondian Group, Ajua Shale Formation, Elmina Sandstone Formation, Petrography, Geochemistry, Provenance, Arkosic arenite, Sub-arkosic arenite

Introduction

The mineral and chemical makeup of siliciclastic sedimentary rocks are influenced by the composition of the rocks they originate from. Factors such as weathering, transportation, climatic conditions and landscape features impact the composition of these source rocks (Armstrong-Altrin et al., 2017, 2015). Consequently, these factors influence the mineral and chemical compositions of siliciclastic rocks (Anani et al., 2018; McLennan et al., 1990). According to a number of researchers, the effective and useful method for evaluating provenance is to combine major oxides and trace elements (Armstrong-Altrin et al., 2014, 2013; Nagarajan et al., 2021). The rocks of the Late Ordovician Ajua Shale and Elmina Sandstone Formations form part of the lower parts of the Sekondian Group of Ghana (Asiedu et al., 2000, 2005; Crow, 1952). Both formations are exposed extensively along the coast of Ghana, from Cape Coast to the mouth of Butre River near the coastal village of Dixcove. The Ajua Shale Formation consists of mainly shales, sandstones and sandy shales while the Elmina Sandstone Formation is made up mainly of sandstones with subordinate shales and conglomerates (Asiedu et al., 2005; Crow, 1952).

Over the years, research work on the Sekondian Group has primarily focused on using major and trace elements, Nd isotopes geochemistry and paleontological evidence to study the provenance, depositional environment, and age of the rocks (Anan-Yorke, 1974; Atta-Peters, 1996, 1999, 2000; Crow, 1952; Mensah, 1973). There has not been a detailed petrographic study of the rocks, which could provide valuable information on the mineralogical and textural to ascertain the provenance of these two formations. Therefore, the objective of this study is to conduct a comprehensive petrographic and geochemical analysis of the sandstones from the Ajua Shale and Elmina Sandstone Formations to determine their provenance and understand the geological history of the Sekondian Group. In order to fill the gaps, new detailed textural and modal mineralogical data of the sandstones of the Ajua Shale and Elmina Sandstone Formations have been obtained. This coupled with geochemistry have been used to constrain the provenance of the Ajua Shale and Elmina Sandstone Formations of the Sekondian Group.

Geology of Study Area

The studied outcrops of the Ajua Shale and Elmina Sandstone Formations are situated along the coast of Ghana from the Elmina-Komenda area all the way to Sekondi-Takoradi area (Figure 1). These are the two lower formations of the Sekon-

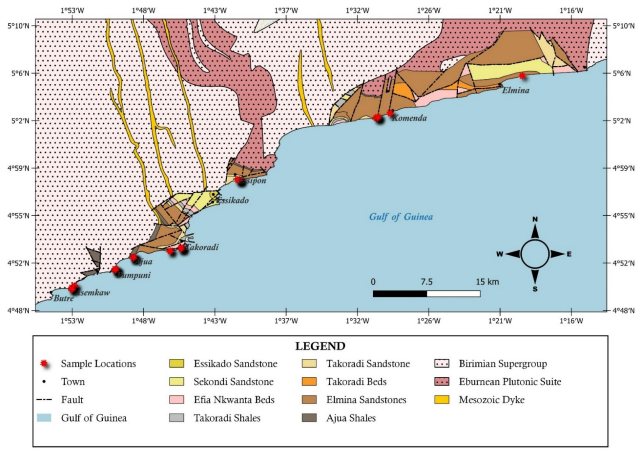

Figure 1. Geological Map of the Sekondian Group Ghana (modified after Asiedu et al. (2005)

dian Group.

Stratigraphically, the Ajua Shale Formation is 60 m thick, the lowest and oldest formation of the Sekondian Group and unconformably overlies the basement complex of the crystalline Birimian rocks. This formation is consists of predominantly dark grey varved shales with flipping laminations of fine to arenaceous material and sandstone beds. Coarse clastic fragments and boulders of rocks of all types including granite, diorite, quartz porphyry and Birimian greenstones embedded in and confined to the shaly portion of the Ajua Shale Formation are observed (Asiedu et al., 2005; Crow, 1952). The Elmina Sandstone Formation, 300 – 400 m thick lies directly on top of the Ajua Shale Formation. The Elmina Sandstone Formation is composed of a uniform medium-grained sandstones that are chocolate in colour and rich in feldspars and mica minerals. Also, the Elmina Sandstone Formation comprises coarse-grained conglomerates at the base and shaly rocks at the top (Asiedu et al., 2005).

Materials and Methods

A total of forty-seven rock samples were collected from the Ajua Shale and Elmina Sandstone Formations along the coastline. Fresh, unweathered and unaltered rock samples were sampled from each location along the stratigraphic column. Twenty sandstone samples each were collected from both the Ajua and Elmina Sandstone Formations and seven sandy shale samples from the Ajua Shale Formation ensuring representative coverage of the lithological variations within each formation. The samples were carefully labeled and their locations were recorded using a handheld GPS device. The samples were then transported to the laboratory for further analyses.

Sample Preparation

To study the mineralogical composition of the rocks, via petrographic observations, thin sections were prepared from 47 rock samples. A slice of each sample was cut, glued with epoxy resin, ground, and polished down to a flat surface of 30μm thickness. The rock thin sections were subsequently viewed under a petrographic microscope, and the constituent minerals were identified and described.

For the XRF and XRD analyses, the samples were crushed, grounded and sieved. First, the rock samples were cut into clean slabs by trimming and removing all dirt, thereby only exposing fresh surfaces only. The cleaned slabs were crushed into smaller pieces and further grounded into powder using the agate mortar and pestle. The grounded samples were then put into a stack of arranged sieves from bottom to top 63 - 500 μm (sieve sizes include 63 μm, 125μm, 250μm, and 500μm). Clearly labelled zip lock sample bags were used to store the various sizes of sieved samples. Fine powder samples of grain sizes of grade 63 μm and 125 μm were used for the XRD and XRF analyses respectively in the laboratories of Department of Earth Science University of Ghana.

Data Analyses

Petrographic and Mineralogical Analysis

Mineralogical composition, texture and microstructures were studied under the petrographic Leica DM750P polarizing microscope coupled with an AmScope camera and Pelcon Point Counter 64 for capturing photos and point counting. Mineral constituents of the rocks were determined by observing the optical properties of the minerals under both Plane Polarized Light (PPL) and Crossed Polarized Light (XPL).

Modal analysis of detrital framework grains was conducted using the Pelcon Point Counter 64 and Gazzi-Dickinson method (Dickinson, 1970; Osae et al., 2006). A minimum of 500 points counted per sandstone rock thin section. Each sandstone rock thin section underwent analysis using an evenly spaced counting grid, systematically traversing the section to tally both framework grains and matrix elements. The grids were positioned to extend beyond grain boundaries, preventing duplicate counts. Minerals within the sandstones were categorized as quartz (both mono and poly crystalline forms), feldspar, lithic fragments, mica and accessories of cement, and matrix. Gazzi-Dickinson's total counts of quartz-feldspar-lithic fragments (Qt-F-L) and (Qm-F-Lt) normalized to 100% (Dickinson, 1970) were utilized in standard sandstone classification and tectonic setting diagrams respectively.

Petrographic data obtained from the thin sections were used to classify the sandstones based on their mineralogical composition, following the classification schemes of Pettijohn (1975) and Baumann et al. (2016). The relative percentages of quartz, feldspar, and lithic fragments were calculated from point counting data and plotted on the ternary diagrams to visualize sandstone compositions using Excel, DeltaGraph7 and CorelDraw2021 softwares.

Powder grain size grade of $<$63 μm was used for the XRD analysis of ten sandstone samples, five each from the Ajua Shale and Elmina Sandstone Formations for their mineralogical composition. The powder samples were mounted onto the XRD glass sample holder of 0.5 mm and analyzed using

the Rigaku MiniFlex600 XRD equipment at the Department of Earth Science University of Ghana. The XRD measurements were carried out the following analytical conditions; an acceleration voltage of 40 Kv; emission current of 15 Ma; scan conditions (scan mode = 0D (continuous); scan axis = $\theta/2\theta$; and scan range = 3^o - 90^o; scan rate = 4.00^o/min; step size = 0.01^o/step). Peak evaluation and phase identification were interpreted using the SmartLab Studio II software and the search and match PDF- 4 Axiom 2022 from the ICDD database.

X-ray diffraction (XRD) data were processed using SmartLab Studio II software and the search and match PDF-4 Axiom 2022 from the ICDD database to identify the mineral phases present in the sandstone samples. The relative abundance of each mineral was estimated based on peak intensities.

Geochemical Analysis

Four grams of powder grain size grade of 125 μm of 40 samples (18 sandstones from the Elmina Sandstone Formation, 15 sandstones and 7 sandy shale samples from the Ajua Shale Formation were used for the whole rock geochemical XRF analysis. The major oxides and trace element analyses were carried out using the Rigaku NexCG XRF machine at the Department of Earth Science, University of Ghana. The XRF analysis was carried out using the following principle and parameters; The X-ray excites the component elements of four secondary targets of Aluminium (Al), Molybdenum (Mo), Copper (Cu) and Rigaku crystal-9 (RX9) with a polychromatic beam being converted to a monochromatic beam by the 3-D Cartesian Geometry (CG) optical kernel. The spectra emitted by sample materials were recorded by a silicon drift detector which produces superior peak shapes and resolution with high throughput. The fundamental parameters (FP) method and analytical conditions of an atmosphere of Helium at a flow rate of 0.660 l/min, tube voltage = 50 kV and tube current = 1.00 mA were employed.

X-ray fluorescence (XRF) data were processed using the Rigaku NexCG XRF fundamental parameters (FP) double determination method. Major element oxides were normalized to 100% on a volatile-free basis. Geochemical data were used to calculate various provenance indicators, such as Chemical Index of Alteration (CIA) and Chemical Index of Weathering (CIW). Tectonic discrimination diagrams and other geochemical plots were used to infer the provenance and tectonic setting of the source rocks. The software programs Excel and CorelDraw2021 were used for final data processing, visualization, and graphical representation.

Results and Discussion

Results

Petrography and Modal Analysis of Sandstones from the Ajua Shale and Elmina Sandstone Formations

The sandstones from the Ajua Shale Formation are generally fine-grained, angular to sub-angular to sub-rounded, moderate to well-sorted and sub-mature. Also, the sandstones from

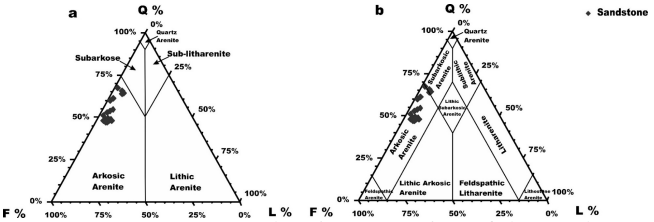

Figure 2. QFL ternary plots interpretation of the sandstone composition from the petrography of the Ajua Shale Formation after (a) Pettijohn (1975) and (b) Baumann et al. (2016) adapted after Dott (1964). Quartz, Feldspar, Lithic grains (Q, F, L), showing (a) Arkosic arenites. (b) Arkosic arenites and few sub-arkosic arenites.

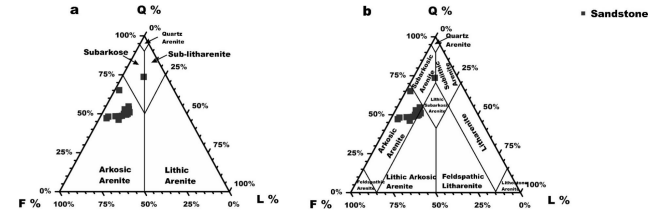

Figure 3. QFL ternary plots interpretation of the sandstone composition from the petrography of the Elmina Sandstones (a) Pettijohn (1975) and (b) Baumann et al. (2016) adapted after Dott (1964). Quartz, Feldspar, Lithic grains (Q, F, L), showing (a) Arkosic arenites and a sub arkose. (b) Arkosic arenites and a sub-arkosic arenite.

the Elmina Sandstone Formation are very fine to fine-grained, sub-angular to sub-rounded, moderate to well- sorted and sub-mature. The sandstones of the Ajua Shale Formation consist of framework grains of monocrystalline (Qm) and polycrystalline quartz (Qp), plagioclase feldspar (Pl) and K-feldspars (microcline (Mc) and orthoclase (Or)), lithic fragments of both sedimentary (Ls) and metamorphic (Lm). Accessory minerals of mica muscovite (Ms), zircons (Zr), matrix (Mx) and opaque minerals (Opq). The sandstone samples of the Elmina Sandstone Formation are made up of framework grains of monocrystalline (Qm) and polycrystalline quartz (Qp), plagioclase feldspar (Pl) and K-feldspars (microcline (Mc)), lithic fragments of both sedimentary (Ls) and metamorphic (Lm). The accessory minerals present are mainly mica minerals of muscovite (Ms) and biotite (Bt), heavy minerals (HM) such as zircons (Zr), opaque minerals (Opq) and matrix (Mx).

The sandstones have been classified based on the modal compositions of their detrital framework grains and matrix contents after Pettijohn (1975) and Baumann et al. (2016). The Ajua Shale and Elmina Sandstone Formations sandstones are classified as mainly arkosic arenite and a few sub-arkosic arenite (Figure 2 and Figure 3) indicating they are slightly mineralogically mature.

Quartz

Ajua Shale Formation

Quartz emerges as the predominant mineral, accounting for approximately 33.8% to 57.6%, with an average of 43.02%, within the framework grains of the sandstones. Within the

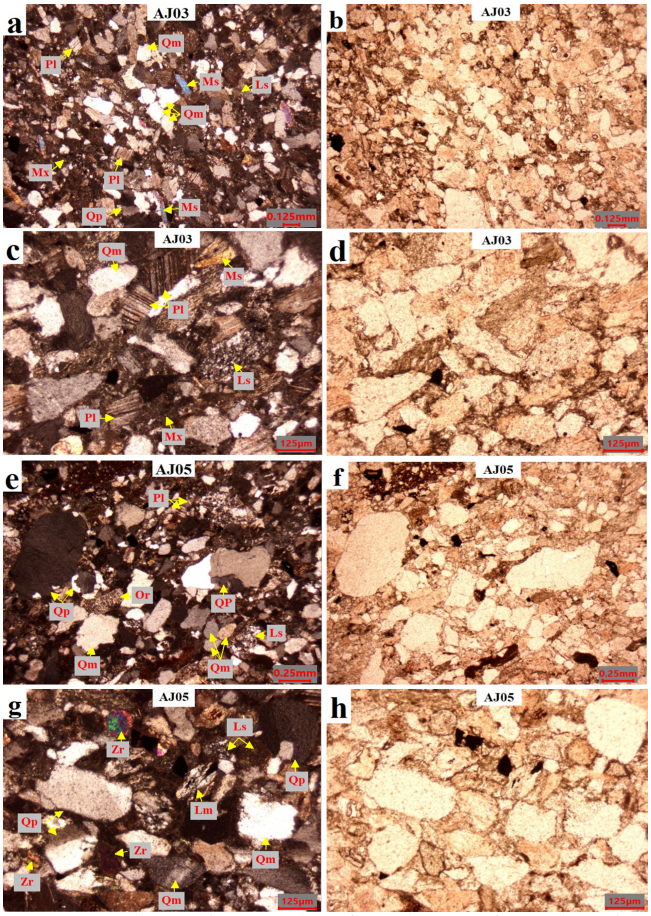

Figure 4. Photomicrographs of sandstones from the Ajua Shale Formation (under cross polars (XPL) and plane polars (PPL)) showing (A) XPL & (B) PPL; fine-grained texture, sub-angular to sub-rounded quartz grains, matrix-supported and moderate to well-sorted mineral grains. (C) XPL & (D) PPL; fresh euhedral feldspar grains of plagioclase and large sub-rounded sedimentary lithic. (E) XPL & (F) PPL; large sub-rounded (2-3) polycrystalline quartz grains and orthoclase feldspar. (G) XPL & (H) PPL; large rounded zircon heavy minerals, metamorphic and sedimentary lithics.

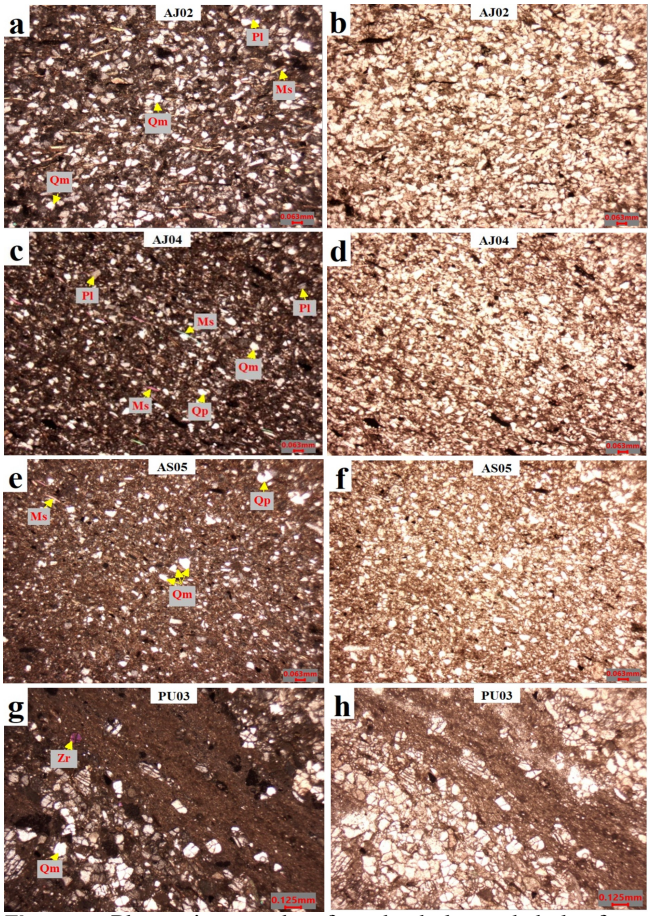

Figure 5. Photomicrographs of sandy shales and shales from the Ajua Shale Formation (under cross polars (XPL) and plan polars (PPL)) showing (a) XPL & (b) PPL: very fine-grained texture, sub-angular to sub-rounded quartz grains, tiny muscovite minerals, matrix-supported and well-sorted mineral grains. (c) XPL & (d) PPL, (e) XPL & (f) PPL; very fine-grained texture, sub-angular to sub-rounded quartz grains, tiny muscovite minerals, matrix-supported and well-sorted mineral grains. (k) XPL & (l) PPL; small rounded heavy minerals, fractured quartz grains and dark brown fine-grained matrix of clay mineral.

Ajua Shale Formation samples, both monocrystalline and polycrystalline quartz grains occur. Monocrystalline quartz being the dominant quartz type constitute about 74% of the quartz grains. Monocrystalline quartz grains are mainly angular to subrounded in shape. The quartz grains display both undulose and non-undulose extinction patterns (Figure 4 and Figure 5). The polycrystalline quartz grains, on the other hand are sub-angular to sub-rounded, medium-grain (0.25 mm) size and exhibit undulose extinction as observed in Figure 4 (a), Figure 4 (e) and Figure 4 (g).

Elmina Sandstone Formation

Quartz takes precedence as the most prevalent mineral, accounting for approximately 33.4% to 65.8%, with an average of 41.1%, among the framework grains found within the sandstones of the Elmina Sandstone Formation. There are both monocrystalline and polycrystalline quartz grains, with monocrystalline quartz being the prevailing type constituting 79% of the quartz grains. These monocrystalline quartz grains display sub-angular to sub-rounded shapes and are characterized by fine grain (0.125 mm) sizes. They also showcase both undulose and non-undulose extinction patterns observed in Figure 6. The texture of the polycrystalline quartz grains, their texture is sub-angular to sub-rounded, and they exhibit a medium-grain size shown in Figure 6 (e) and Figure 6 (g).

Feldspar

Ajua Shale Formation

Feldspars content range from 24.0% to 38.8%, with an average of 33.2%, of the detrital framework in the sandstones of the Ajua Shale Formation. Among the feldspar minerals

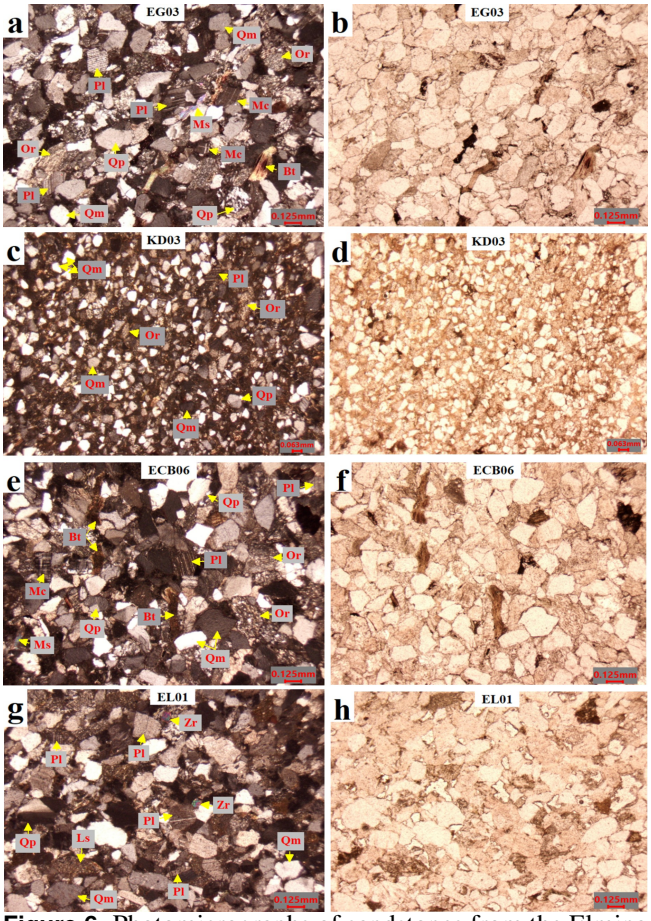

Figure 6. Photomicrographs of sandstones from the Elmina sandstone Formation (under cross polars (XPL) and plane polars (PPL)) showing (a) XPL & (b) PPL; fine-grained texture, sub-angular to sub-rounded quartz grains, grain-supported and moderate to well-sorted mineral grains. (c) XPL & (d) PPL; very fine-grained texture, sub-angular to sub-rounded quartz grains, matrix-supported and moderate to well-supported mineral grains. (e) XPL & (f) PPL; fresh euhedral feldspar grains of microcline and plagioclase and orthoclase. (g) XPL & (h) PPL; fresh euhedral feldspar grains of plagioclase, and some zircon heavy minerals.

observed in the sandstones, both plagioclase feldspar and alkali feldspar (microcline and orthoclase) are prominent, with the alkali feldspar being the prevailing type constituting about 54 % of the feldspar minerals. These feldspars exhibit euhedral forms, characterized by fine grain (0.125 mm) sizes and demonstrate a fresh state with minimal to no evident alteration (evident Figure 4 (c) and Figure 4 (e)).

Elmina Sandstone Formation

Feldspars constitute a range of approximately 10.8% to 41.8%, with an average of 27.62%, of the overall framework grains found within the sandstones of the Elmina Formation. In these sandstones, both plagioclase feldspar and alkali feldspar (microcline and orthoclase) are prevalent feldspar minerals, with plagioclase being the dominant variety of about 77%. These feldspar minerals showcase euhedral forms, and their grain sizes range from fine to medium (0.125 – 0.25 mm). They also appear to be in a fresh state, displaying minimal to no signs of alteration as shown in Figure 6 (a) and Figure 6 (e).

Lithic Fragments

Ajua Shale Formation

In the sandstones of the Ajua Shale Formation, lithic fragments emerge as the third predominant component within the framework grains, accounting for approximately 1.2% to 5.8%, with an average of 3.77%, in the sandstones of the Ajua Shale Formation. The lithic fragments identified in these sandstones encompass both sedimentary and metamorphic varieties (Figure 4 (c) and Figure 4 (g)). Among these, the sedimentary lithic fragments are predominantly comprised of chert. These fragments bear evidence of recycling, originating from sedimentary or metamorphic rocks that have undergone erosion, resulting in their reduction to smaller, sand-sized grains, which are now present in the sandstone samples. The metamorphic lithics are also predominantly composed of quartz showing planar fabric of mineral orientation in a preferred direction.

Elmina Sandstone Formation

In the Elmina sandstones, lithic fragments constitute the third most prominent component among the framework grains, encompassing approximately 0.2% to 11.6%, with an average of 7.84%, within the Elmina sandstones. The lithic fragments present in this formation comprises both sedimentary and metamorphic varieties as shown in Figure 6 (g).

Accessory Minerals

Ajua Shale Formation

The accessory minerals observed in the sandstone and shaly samples include; mica of muscovite and some heavy and opaque minerals. Accessory minerals in the sandstones constitute about 2.8% - 11.4%, averaging of 6.69% of the total framework mineral grains. The detrital muscovite grains ranging from (1.2% - 3.8%, average = 2.67%) are distinguished by their elongated fiber-like appearance and high birefringence as shown Figure 4 (a) and Figure 4 (c). The heavy minerals of zircon are less abundant (0.6% - 3.8%, average = 2.07%) compared to the muscovite minerals and are observed as individual grains in the matrix of the rocks as seen in Figure 4 (g). The opaque minerals appear as dark subhedral to euhedral grains in the rocks as observed in Figure 4.

Elmina Sandstone Formation

The accessory minerals observed in the Elmina sandstone samples include; mica of biotite and muscovite, some heavy and opaque minerals. They make up about 0.8 % - 11.2 %, average of 7.53 % of the entire rock. The biotite minerals appear as brown lathlike grains ranging from 0.2% - 3.4%, (average = 1.87%) seen in Figure 6 (e). Also, the muscovite minerals ranging from 2.0% -4.6%, (average = 2.93%) are

Table 1. Whole Rock Geochemistry of Sandstone and Sandy Shale Samples from the Ajua Shale Formation

	Sandstones											Sandy Shales									
SAMPLE ID	AJ01	AJ03	AJ06	AJ09	AS01	AS02	AS03	AS06	AS07	AS08	PU01	PU03	PU04	PU08	PU10	AJ02	AJ04	AJ10	AS04	AS05	AS09	PU11
MO (Wt. %)																						
SiO_2	69.300	67.700	66.200	71.200	74.400	80.200	76.900	74.200	67.900	79.500	69.500	64.000	71.100	69.000	65.500	62.200	63.200	59.700	64.200	62.200	64.000	65.900
TiO_2	0.417	0.549	0.590	0.376	0.710	0.675	0.458	0.227	0.522	0.771	0.477	0.660	0.371	0.461	0.557	0.706	0.696	0.707	0.828	0.860	0.683	0.845
Al_2O_3	13.900	14.400	12.400	13.400	11.800	9.970	10.400	12.500	14.400	10.000	14.700	16.000	13.300	13.400	15.900	15.100	16.100	16.100	16.200	16.500	15.200	15.800
Fe_2O_3	3.820	4.200	4.030	3.440	2.730	2.760	2.690	1.830	4.070	2.560	3.630	5.120	3.580	3.670	3.870	6.250	5.500	7.250	6.160	6.890	5.730	6.650
MnO	0.069	0.080	0.154	0.066	0.049	0.073	0.059	0.046	0.083	0.071	0.070	0.088	0.072	0.093	0.109	0.108	0.091	0.129	0.112	0.122	0.109	0.097
MgO	3.980	3.870	3.390	2.860	1.990	1.320	2.980	2.150	3.490	1.320	3.130	4.320	3.450	2.800	3.420	4.920	4.680	6.040	4.730	5.180	4.540	4.130
CaO	0.917	1.110	6.450	0.904	1.130	0.623	0.381	2.380	1.800	0.588	1.570	1.730	0.715	3.160	3.430	1.850	1.720	1.550	1.570	1.700	2.240	1.810
Na_2O	5.640	5.880	5.110	5.900	3.960	2.520	4.120	4.250	5.600	3.110	4.820	4.950	5.610	5.740	4.940	4.880	4.940	4.190	2.980	2.980	4.420	2.490
K_2O	1.490	1.620	1.270	1.390	1.920	1.200	1.540	1.700	1.510	1.460	1.600	2.060	1.410	1.210	1.750	2.090	1.960	2.240	2.700	2.780	2.380	1.750
P_2O_5	<0.006	<0.007	<0.006	<0.006	<0.729	<0.009	<0.007	<0.005	<0.007	<0.009	<0.007	<0.008	<0.006	<0.007	<0.008	<0.084	<0.074	<0.005	<2.280	<1.750	<0.008	<0.008
SrO	0.014	0.018	0.015	0.015	0.021	0.017	0.011	0.021	0.023	0.016	0.020	0.028	0.013	0.015	0.025	0.024	0.024	0.022	0.020	0.021	0.025	0.010
BaO	0.038	0.043	0.031	0.037	0.037	0.023	0.022	0.103	0.079	0.020	0.047	0.051	0.035	0.029	0.053	0.043	0.042	0.049	0.060	0.047	0.055	0.044
TOTAL	99.550	99.430	99.610	99.550	98.710	99.360	99.538	99.300	99.397	99.400	99.520	98.956	99.622	99.549	99.501	98.250	99.027	97.980	101.800	101.030	99.390	99.530
CP**																						
SiO_2/Al_2O_3	4.986	4.701	5.339	5.313	6.305	8.044	7.394	5.936	4.715	7.950	4.728	4.000	5.346	5.149	4.119	4.119	3.926	3.708	3.963	3.770	4.211	4.171
K_2O/Na_2O	0.264	0.276	0.249	0.236	0.485	0.476	0.374	0.400	0.270	0.469	0.332	0.416	0.251	0.211	0.354	0.236	0.261	0.352	0.596	0.614	0.354	0.462
CIA	52.560	51.770	40.560	51.070	56.996	60.330	53.278	48.740	50.522	56.360	54.040	54.238	52.485	44.846	49.535	53.580	54.950	57.040	75.610	70.766	52.232	63.050
CIW	55.980	55.250	42.470	54.170	63.355	65.480	58.252	52.510	53.595	61.870	57.720	58.672	55.848	46.902	52.642	57.440	59.239	62.400	87.550	81.252	57.305	68.200
PIA	52.920	52.020	39.630	51.200	58.753	62.260	53.953	48.530	50.590	57.740	54.630	54.992	52.825	44.351	49.473	54.130	55.788	58.510	85.220	77.991	52.713	65.370
ICV	1.175	1.202	1.693	1.115	1.058	0.920	1.176	1.007	1.186	0.988	1.041	1.183	1.144	1.279	1.137	1.378	1.217	1.373	1.178	1.243	1.323	1.125
SAMPLE ID	AJ01	AJ03	AJ06	AJ09	AS01	AS02	AS03	AS06	AS07	AS08	PU01	PU03	PU04	PU08	PU10	AJ02	AJ04	AJ10	AS04	AS05	AS09	PU11
TE* (ppm)**																						
Mn	527.000	710.500	1330.000	546.000	384.000	496.000	454.000	404.000	670.000	544.000	495.000	686.500	583.000	705.500	833.000	1025.000	806.500	1170.000	1015.000	1090.000	931.500	767.500
V	52.300	85.400	87.400	57.500	100.000	83.000	58.000	53.000	79.900	90.300	59.700	81.800	57.500	63.200	83.200	119.000	127.000	126.000	164.000	179.000	127.000	138.000
Cr	28.800	64.000	51.400	29.300	63.100	56.900	38.300	19.800	45.100	71.700	43.800	72.000	25.700	42.100	48.600	109.000	91.100	92.600	116.000	131.000	82.800	87.800
Co	46.500	65.900	62.400	52.800	27.900	8.500	23.300	16.100	64.100	-	39.100	76.200	41.100	33.400	48.800	137.000	109.000	160.000	140.000	138.000	112.000	124.000
Ni	21.800	35.100	25.700	18.700	17.100	25.500	17.600	17.800	26.700	27.800	23.200	35.100	20.800	25.700	25.100	49.400	43.600	52.600	55.300	56.000	46.700	41.600
Cu	12.700	23.000	16.100	14.600	36.100	9.850	20.600	21.100	20.300	8.940	18.500	23.400	11.170	12.900	19.100	43.600	33.900	51.400	49.900	42.000	39.100	32.400
Rb	33.200	45.200	34.200	33.600	44.500	30.400	36.900	42.200	39.200	32.400	36.200	56.700	31.600	28.600	42.100	73.700	63.900	79.700	97.200	104.000	81.200	46.600
Sr	116.000	173.000	144.000	130.000	165.000	118.000	91.700	181.000	196.000	125.000	148.000	227.000	111.000	119.000	197.000	245.000	233.000	225.000	196.000	200.000	234.000	182.000
Ba	336.000	446.000	309.000	353.000	303.000	171.000	204.000	976.000	752.000	179.000	403.000	469.000	328.000	263.000	483.000	475.000	443.000	540.000	648.000	504.000	552.000	393.000
Y	20.300	25.300	29.100	18.700	32.500	22.200	15.600	17.100	25.100	23.400	18.300	24.100	18.400	21.700	23.900	34.300	30.100	27.800	41.600	50.100	26.500	33.900
Zr	2045.000	2317.000	2595.000	2159.000	2268.000	2470.000	2020.000	2105.000	2272.000	2780.000	2007.000	2184.000	2220.000	2120.000	2370.000	2537.000	2307.000	2472.000	2482.000	2564.000	2398.000	2562.000
Hf	-	27.800	30.100	-	23.000	27.600	15.200	-	25.100	32.200	13.600	29.000	20.900	18.300	25.700	-	18.100	-	-	15.400	26.300	22.500
Nb	12.700	10.390	17.200	7.880	11.300	11.400	-	-	9.870	14.800	10.740	13.500	-	12.300	12.600	20.200	20.500	16.400	20.900	18.200	15.400	17.700
Ta	20.200	23.600	16.700	18.500	19.200	20.000	21.500	13.880	27.000	27.200	21.100	25.700	23.800	27.900	28.300	28.200	31.900	28.100	19.900	27.900	27.400	27.700
Pb	11.200	21.800	8.890	10.600	14.800	10.210	11.600	11.300	13.000	11.500	11.200	20.000	9.210	7.710	12.400	28.800	22.100	32.200	14.600	12.600	14.400	11.800
Zn	43.200	57.300	50.700	40.900	35.200	38.700	31.200	28.000	52.900	41.500	38.600	68.600	42.300	43.400	43.800	96.300	85.200	116.000	99.100	108.000	87.300	83.700
Sn	17.800	18.900	21.300	18.200	19.400	16.700	17.800	19.500	17.000	19.300	18.000	18.700	16.700	18.600	18.800	19.800	18.600	23.300	20.100	21.400	20.100	19.000
Ga	10.460	11.300	14.300	9.560	6.950	5.370	4.920	7.060	8.830	5.110	6.980	11.600	8.600	7.550	8.600	16.500	12.800	19.100	19.400	18.700	14.500	12.400
As	-	7.590	1.890	0.937	8.190	5.090	5.680	0.406	1.280	5.830	2.440	3.970	0.064	1.380	2.040	14.100	4.890	11.300	6.690	6.480	5.580	2.820
Th	7.030	9.890	9.600	7.050	9.980	7.740	6.930	-	-	8.680	7.530	9.910	7.180	7.210	8.680	13.100	11.500	12.900	12.300	11.900	10.390	10.800

CIA = Chemical Index of alteration (Nesbitt and Young, 1982) and PIA = plagioclase index of alteration (Fedo et al., 1995) calculated following the procedure given in Fedo et al. (1995). ICV= index of chemical variability. MO* = Major Oxides, CP** = Chemical Parameters, TE*** = Trace Elements.

distinguished by their elongated fiber-like appearance and high birefringence as seen in Figure 6 (a). The heavy minerals, mainly zircons as shown in Figure 6 (g) are less abundant ranging from 0.2% - 3.4%, (average = 1.16%) compared to the mica minerals and are observed as individual grains in the matrix of the rocks.

Matrix and Cement

Ajua Shale Formation

The detrital framework grains of within the analyzed sandstone samples are enclosed by a matrix, comprises of approximately 8.6% to 19.4%, with an average of 13.3%, of the overall rock composition. The matrix is primarily characterized by dark brown clay minerals, a prevalent feature in both the sandstones and sandy shale samples as seen in Figure 4 (a) and Figure 5. Notably, the binding agents that consolidate the framework grains are predominantly composed of silica.

Elmina Sandstone Formation

The framework grains of the examined samples are surrounded by a matrix, accounting for approximately 4.6% to 25.0%, with an average of 16.28%, of the overall composition of the rock. Among the major matrix types observed in the studied samples, dark brown clay minerals predominate as shown in Figure 6 (a). These clay minerals can originate either from detrital sources or as a result of diagenesis. Matrix minerals that have undergone diagenetic modifications are created through changes and the subsequent formation of framework grains, as well as the recrystallization of other components within the matrix. Meanwhile, the binding agents that consolidate the framework grains are primarily composed of silica.

Geochemistry

The major and trace element concentrations of fifteen sandstone and seven sandy shale samples from the Ajua Shale Formation and eighteen sandstones from the Elmina Sandstone Formation are presented (Table 1 and Table 2).

Geochemistry of the Ajua Shale Formation

Major Oxides

Major element distribution patterns reflect the mineralogy of the studied samples. Using the geochemical classification diagram of Herron (1988) Figure 7, the Ajua Shale sandstone units are chiefly classified as wackes and litharenite indicating sub-matured sediments while the sandy shale units are classified as shales.

The sandstones and sandy shale samples show relatively variable compositions characterized by high SiO_2 and Al_2O_3 contents. The sandstone samples have higher SiO_2 content than the associated sandy shale samples. The sandy shale samples are enriched in Al_2O_3 (15.1 % to 16.5 %, average = 15.86 %), K_2O (1.75 % to 2.78 %, average = 2.27 %), Fe_2O_3 (5.5 % to 7.25 %, average = 6.35 %) and TiO_2 (0.70 % to 0.85 %, average = 0.76 %) contents in comparison with those of the sandstones, reflecting their higher clay content. Generally, the Ajua Shale sandstones are rich in SiO_2 content of (65.5 % to 82.2 %, average = 71.1 %) and Al_2O_3 of (10 % to 15.9 %, average = 13.01 %) and low concentrations of Fe_2O_3 (1.83 % to 5.2 %, average = 3.47 %), MgO (1.32 % to 3.98 %, average = 2.96 %), K_2O (1.2 % to 2.06 %, average = 1.54 %) and TiO_2

Table 2. Whole Rock Geochemistry of Sandstones Samples from the Elmina Sandstone Formation

SAMPLE ID	ECB01	ECB02	ECB02A	ECB03	ECB04	ECB05	ECB06	ECB07	EG01	EG02	EG03	EG04	EG05	EG06	EG07	EL01	KD03	KD04
MO* (Wt. %)																		
SiO_2	55.700	57.400	59.300	61.300	58.100	59.200	56.500	56.100	69.300	65.600	69.800	59.400	66.500	67.500	65.100	70.100	63.500	68.900
TiO_2	0.890	0.521	0.567	0.665	0.535	0.548	0.741	0.702	0.496	0.653	0.455	0.548	0.473	0.519	0.692	0.303	0.704	0.466
Al_2O_3	16.000	17.900	18.700	18.100	16.600	17.600	19.000	18.400	14.400	15.500	14.200	14.300	15.100	15.100	15.200	12.700	22.200	13.900
Fe_2O_3	3.970	4.760	7.140	7.650	2.870	2.850	5.130	5.610	3.430	4.870	3.990	4.680	3.940	4.110	6.290	2.050	6.850	3.400
MnO	0.225	0.215	0.135	0.111	0.327	0.201	0.214	0.221	0.103	0.103	0.073	0.118	0.108	0.076	0.098	0.065	0.081	0.161
MgO	3.100	3.150	3.300	3.450	2.340	3.000	2.980	3.080	3.010	4.450	2.890	4.500	3.900	3.410	4.050	1.680	2.360	2.900
CaO	15.000	10.500	5.550	2.500	13.400	10.300	10.600	11.200	0.500	0.770	0.407	9.630	1.630	0.408	0.415	3.500	0.426	0.901
Na_2O	1.670	2.030	1.760	2.250	1.950	2.170	1.200	0.869	6.520	5.600	5.480	4.760	5.890	6.640	4.590	6.690	0.293	6.040
K_2O	2.670	2.940	2.930	3.200	3.130	3.470	2.990	3.010	1.730	1.890	2.240	1.540	1.910	1.770	3.040	2.340	3.070	2.730
P_2O_5	<0.006	<0.006	<0.005	<0.006	<0.006	<0.006	<0.005	<0.005	<0.006	<0.007	<0.006	<0.007	<0.006	<0.006	<0.006	<0.007	<0.008	<0.007
SrO	0.018	0.016	0.016	0.019	0.016	0.016	0.015	0.015	0.010	0.014	0.011	0.017	0.014	0.012	0.013	0.020	0.013	0.019
BaO	0.061	0.065	0.067	0.087	0.066	0.070	0.062	0.064	0.076	0.112	0.056	0.081	0.117	0.068	0.074	0.109	0.088	0.099
TOTAL	99.304	99.497	99.466	99.332	99.334	99.425	99.432	99.271	99.575	99.562	99.601	99.574	99.582	99.613	99.562	99.560	99.292	99.516
CP**																		
SiO_2/Al_2O_3	3.481	3.207	3.171	3.387	3.500	3.364	2.974	3.049	4.813	4.232	4.915	4.154	4.404	4.470	4.283	5.520	2.860	4.957
K_2O/Na_2O	1.599	1.448	1.665	1.422	1.605	1.599	2.492	3.464	0.265	0.338	0.409	0.324	0.324	0.267	0.662	0.350	10.478	0.452
CIA	65.654	64.510	67.633	62.518	62.903	61.794	72.597	75.086	51.632	55.078	53.860	45.236	50.661	52.673	56.754	38.970	83.873	48.921
CIW	74.438	72.827	76.356	70.973	72.125	71.141	82.795	86.551	55.311	59.359	59.278	47.729	54.409	56.417	64.666	42.240	95.838	54.565
PIA	70.521	68.828	72.882	66.455	67.361	66.019	80.022	84.173	51.885	55.941	54.730	44.674	50.767	53.085	58.954	36.940	95.230	48.638
ICV	1.720	1.347	1.143	1.095	1.479	1.281	1.256	1.342	1.097	1.183	1.094	1.803	1.182	1.121	1.262	1.309	0.621	1.194
SAMPLE ID	**ECB01**	**ECB02**	**ECB02A**	**ECB03**	**ECB04**	**ECB05**	**ECB06**	**ECB07**	**EG01**	**EG02**	**EG03**	**EG04**	**EG05**	**EG06**	**EG07**	**EL01**	**KD03**	**KD04**
TE* (ppm)**																		
Mn	1295.000	1455.000	846.000	659.500	2395.000	101.500	1290.000	1335.000	863.500	834.000	575.000	939.500	845.000	642.000	737.500	591.500	562.000	1195.000
Sc	<111.000	<88.800	<50.200	32.500	<120.500	<1520.000	<82.700	<90.300	<19.000	<23.050	<18.050	<101.500	<30.000	<18.050	<18.600	<49.350	<17.550	<22.500
V	88.000	37.200	20.200	36.700	49.900	58.900	39.000	52.500	58.600	70.900	65.400	71.400	58.100	52.300	45.100	57.600	96.500	45.700
Cr	51.200	29.400	40.400	36.600	32.800	29.000	33.700	34.700	45.900	70.000	44.900	53.800	32.800	51.500	74.100	29.000	60.400	30.000
Co	42.200	52.000	70.100	73.900	25.700	27.700	47.700	52.400	46.900	77.800	55.500	64.900	54.800	72.300	91.700	36.100	72.300	49.300
Ni	33.000	36.000	31.900	28.600	35.300	35.900	35.700	36.300	48.200	61.800	58.900	50.500	52.600	33.400	64.500	35.000	24.300	38.000
Cu	23.300	31.900	25.600	10.760	21.200	45.000	25.700	26.600	21.400	19.800	21.500	35.500	23.200	22.900	24.200	18.100	14.000	20.400
Rb	78.700	89.600	92.300	89.100	97.000	95.300	88.200	87.500	58.500	62.900	76.000	57.100	62.400	58.200	113.000	68.200	61.500	71.100
Sr	108.000	113.000	102.000	110.000	126.000	127.000	93.900	93.900	89.600	114.000	93.000	142.000	117.000	106.000	102.000	190.000	89.600	150.000
Ba	422.000	516.000	485.000	594.000	571.000	612.000	456.000	459.000	730.000	1081.000	528.000	778.000	1066.000	650.000	681.000	1112.000	676.000	920.000
Y	29.000	25.000	20.600	17.800	29.300	30.600	21.500	22.600	31.500	37.100	40.400	45.200	30.000	21.200	21.800	56.500	33.200	47.300
Zr	2310.000	2233.000	2176.000	2267.000	2392.000	2288.000	2181.000	2203.000	2105.000	2319.000	2062.000	2448.000	2140.000	2128.000	2199.000	2348.000	2470.000	2105.000
Hf	26.100	21.800	-	23.700	-	20.800	20.400	-	-	27.700	-	-	-	-	21.300	25.400	29.500	-
Nb	16.600	-	10.200	14.300	-	10.500	10.400	11.900	13.500	19.100	12.200	18.500	9.550	11.500	13.400	6.640	13.100	12.300
Ta	22.900	24.500	22.700	32.100	25.200	32.100	24.900	18.000	17.600	25.200	16.700	25.200	21.600	19.000	21.300	30.200	27.400	21.000
Pb	9.620	9.780	12.200	12.200	8.950	13.600	8.130	7.850	17.500	16.600	18.700	15.400	14.000	15.300	20.500	13.400	9.930	12.900
Zn	48.000	54.400	52.200	44.600	54.600	58.700	54.600	51.000	55.100	71.400	64.000	66.300	60.800	54.000	78.400	41.400	37.900	64.900
Ga	14.000	12.900	16.100	10.400	10.300	13.500	14.200	15.600	9.870	13.100	12.000	15.100	11.800	12.400	14.300	8.680	10.310	11.980
Sn	17.800	20.200	18.500	15.600	16.900	18.700	17.400	21.100	18.200	17.900	18.000	21.900	19.000	15.500	17.700	20.400	17.200	16.500
As	0.548	0.193	1.260	0.576	0.177	1.190	1.247	1.470	-	-	1.015	0.847	1.300	0.475	3.050	-	3.420	1.510
Th	13.600	9.430	9.460	10.800	9.660	10.900	10.040	10.700	11.300	13.100	9.000	10.300	10.280	9.630	9.650	10.700	14.300	12.200

CIA = Chemical Index of alteration (Nesbitt and Young, 1982) and PIA = plagioclase index of alteration (Fedo et al., 1995) calculated following the procedure given in Fedo et al. (1995). ICV= index of chemical variability. MO* = Major oxides, CP** = Chemical Parameters, TE*** = Trace element

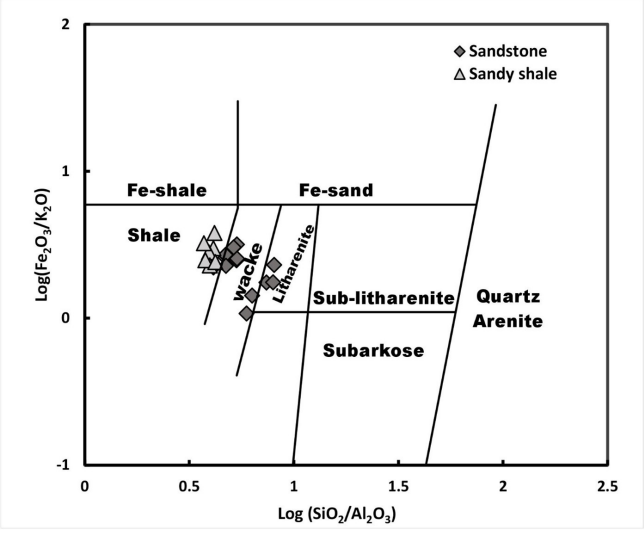

Figure 7. Geochemical classification plot of siliciclastic rocks (sandstones and sandy shales) of the Ajua Shale Formation after Herron (1988), showing $Log(Fe_2O_3/K_2O)$ versus $Log(SiO_2/Al_2O_3)$

of (0.23 % to 0.71 %, average = 0.52 %) as compared to those of the sandy shale samples. The sandy shales possess SiO_2 content of (59.7 % to 65.9 %, average = 63.1 %) and Al_2O_3 of 15.1 % to 16.5 %, (average = 15.9 %). Also, an increasing variation in the concentration values of Fe_2O_3 of (5.5 % to 7.3 %, average = 6.3 %), MgO of (4.1 % to 6.04 %, average = 4.9 %), K_2O of (1.8 % to 2.8 %, average = 2.3 %), TiO_2 of (0.68 % to 0.86 %, average = 0.76 %) and P_2O_5 (<0.005 % to 0.009 %) less than 1 % were observed.

The concentration values of Na_2O and CaO obtained d in the sandstones ranges from 2.52 % to 5.88 %, (average = 4.81 %) and 0.381 % to 3.43 %, (average = 1.79 %) respectively while in the sandy shale they range from 2.49 % to 4.94 %, (average = 3.84 %) and 1.55 % to 2.24 %, (average = 1.77 %) respectively.

Averages of major element concentrations of the Ajua Shale Formation sandstones and sandy shales were normalized against the average PAAS data representative of continentally derived sediments Taylor and McLennan (1985) as shown in the spider diagram plots (Figure 8). By comparison with average Post Archean Australian Average Shale (PAAS), the Ajua Shale sandstone samples normalized against PAAS show enrichment in SiO_2, MgO, CaO and Na_2O, depletion in TiO_2, Al_2O_3, Fe_2O_3, CaO, MnO, K_2O, and P_2O_5 (Figure 8). The Ajua Shale sandy shale samples normalized against PAAS show enrichment in SiO_2, MnO, MgO, CaO, Na_2O and P_2O_5, depletion in TiO_2, Al_2O_3, Fe_2O_3 and K_2O as shown in (Figure 8).

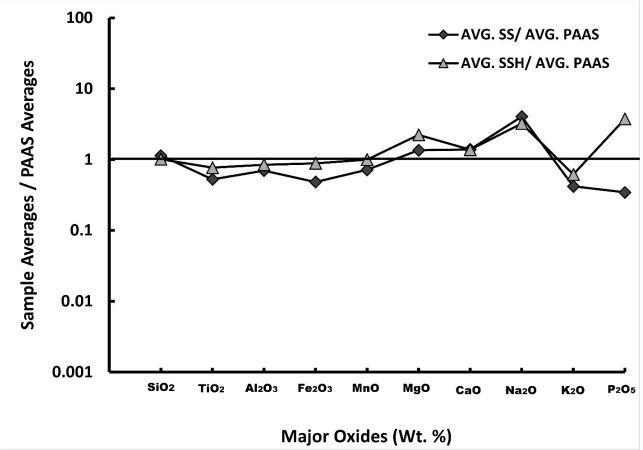

Figure 8. Spider plot showing averages of major element concentrations of the Ajua Shales Formation sandstones (AVG. SS) and sandy shale (AVG. SSH) samples normalized a gainst average PAAS (AVG.PAAS) data (after Taylor and McLennan (1985)).

Trace elements

The analyzed sandstone and sandy shale samples from the Ajua Shale Formation show significant variations in trace elements as shown in Table 1. In the sandstones and shales, the contents of large ion lithophile elements (LILE; Rb, Ba, Sr and Th) range from 28.6 ppm to 104 ppm, 171 ppm to 976 ppm, 91.7 ppm to 245 ppm, and 6.93 ppm to 13.1 ppm respectively. The content of high field strength elements (HFSE; Zr, Hf, Nb, Ta and Y) range from 2007 ppm to 2780 ppm, 9.1 ppm to 35 ppm, 13.6 ppm to 30.1 ppm, 7.9 ppm to 14.8 ppm, and 16.7 ppm to 31.9 ppm respectively. Similarly, transition trace elements (TTE; Mn, Sc, Cr, V, Co, Ni, Cu and Zn) range from 404 ppm to 1330 ppm, 17 ppm to 68.7 ppm, 19.8 ppm to 131 ppm, 52.3 ppm to 179 ppm, 8.5 ppm to 160 ppm, 17.1 ppm to 56 ppm, 8.9 ppm to 51.4 ppm and 28 ppm to 116 ppm respectively. Generally, the sandy shales have higher concentrations of the LILEs and TTEs than the sandstones. On the other hand, the sandstones have higher concentrations of Hf and Zr than the sandy shales. Averages of trace element concentrations of the Ajua Shale Formation sandstones and sandy shales were normalized against the average PAAS data Taylor and McLennan (1985) as shown in the spider diagram plot (Figure 9). Trace elements (Zr, Hf, Sc and Co) show significant enrichment in both lithotypes relative to PAAS. The strong enrichment of Zr and Hf is likely associated with the presence of zircon minerals.

Relative to PAAS, the sandstones are depleted in the LILEs, Y and Nb, and TTEs except for Sc and Co (Figure 9). The sandy shales are enriched in Sr, Y, and the TTEs relative to PAAS except for V, Cu and Ni relative to PAAS. Also, relative to PAAS the sandy shales are also depleted in Rb, Ba, Th, Nb, V, Cu and Ni. Depletion of the LILEs Rb and Ba in both lithotypes are mainly controlled by clay minerals. Depletion of Sr in the sandstone samples is probably related to feldspar weathering that is easily mobilized and absorbed onto clay minerals. Also, the enrichment of Sc and slight depletion of

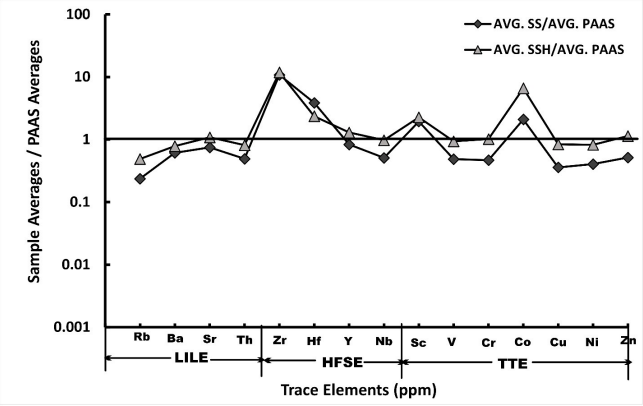

Figure 9. Spider plot showing averages of trace element concentrations of the Ajua Shale Formation sandstones (AVG. SS) and shales (AVG. SSH) normalized a gainst average PAAS (AVG.PAAS) data (after Taylor and McLennan (1985)).

Ni observed in the sandy shales compared to PAAS can be attributed to presence of the phyllosilicates.

Geochemistry of the Elmina Sandstone Formation

Major Oxides

Using the geochemical classification diagram of Herron (1988) (Figure 10), the sandstones from the Elmina Sandstone Formation are chiefly classified as shales, wackes, sub-litharenite and sub-arkose indicating sub-matured sediments.

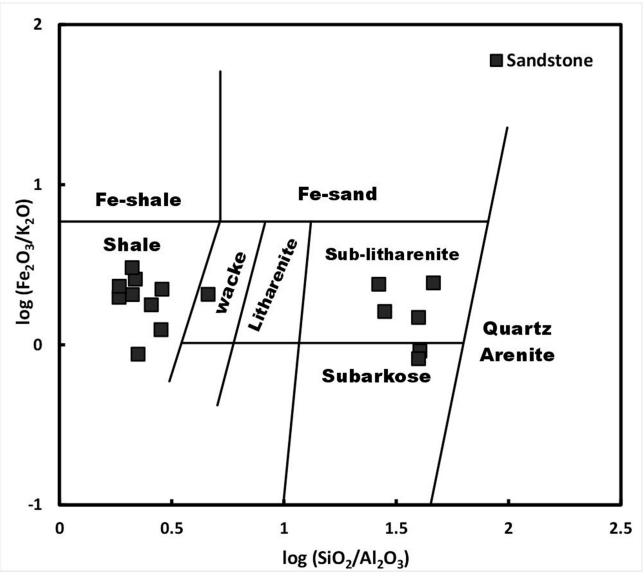

Figure 10. Geochemical classification of siliciclastic rocks (sandstones) from the Elmina Sandstone Formation using the Herron (1988) diagram, showing $\log(Fe_2O_3/K_2O)$ versus $\log(SiO_2/Al_2O_3)$.

Generally, the sandstones of the Elmina Sandstone Formation are characterized by high SiO_2 and Al_2O_3 contents. A significant variation of SiO_2 observed in the sandstones ranges from 55.7 % to 70.1 % (average = 62.69 %), and Al_2O_3 content ranges from 12.7 % to 18.7 % (average = 16.04 %). Low concentrations are recorded for CaO (0.407 % to 15 %, average = 5.72 %), Fe_2O_3 (2.05 % to 7.65 %, average = 4.51 %),

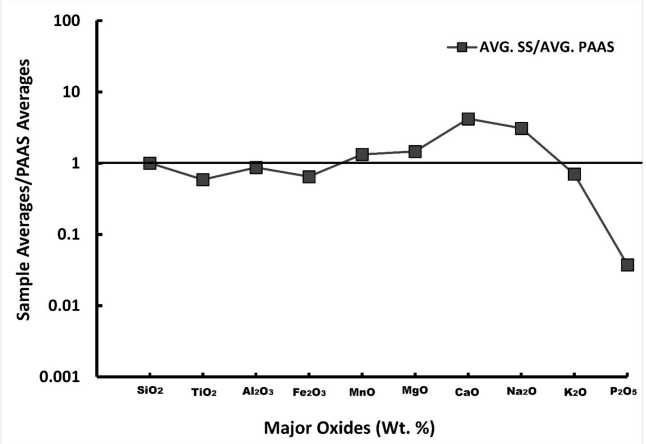

Figure 11. Spider plot showing averages of major element concentrations of the Elmina Sandstone Formation sandstones (AVG. SS) normalized against average PAAS (AVG. PAAS) data, (after Taylor and McLennan (1985)).

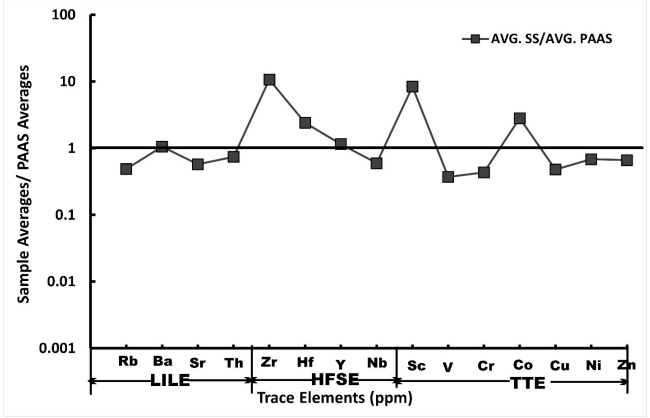

Figure 12. Spider plot showing averages of trace element concentrations of the Elmina Sandstone Formation sandstones (AVG. SS) normalized against average PAAS (AVG. PAAS) data, (after Taylor and McLennan (1985)).

MgO (1.68 % to 4.45 %, average = 3.25 %), K_2O (1.54 % to 3.47 %, average = 2.56 %) and Na_2O (0.87 % to 6.69 %, average = 3.89 %). TiO_2 and MnO concentrations are relatively lower than 1 %.

Averages of major element concentrations of the Elmina Sandstone Formation sandstones were normalized against the average PAAS data representative of continentally derived sediments by Taylor and McLennan (1985), as shown in the spider diagram plots (Figure 11). By comparing with the average Post-Archean Australian Shale (PAAS), the Elmina Sandstone samples normalized against PAAS show depletion in TiO_2, Al_2O_3, Fe_2O_3, K_2O and P_2O_5 (Figure 10). Also, an enrichment pattern is observed in MnO, MgO, CaO, Na_2O, and a slight enrichment in SiO_2 relative to PAAS (Figure 11).

Trace Elements

The analyzed sandstone samples from the Elmina Sandstone Formation show several variations in trace element concentrations, as presented in Table 2. In the sandstones, the contents of large ion lithophile elements (LILE; Rb, Ba, Sr, and Th) range from 58.2 to 113 ppm, 422 to 1112 ppm, 89.6 to 190 ppm, and 9 to 14.3 ppm, respectively. The contents of high field strength elements (HFSE; Zr, Hf, Nb, Ta, and Y) range from 2062 to 2470 ppm, 20.4 to 29.5 ppm, 6.4 to 19.1 ppm, 16.7 to 32.1 ppm, and 17.8 to 56.5 ppm, respectively. Similarly, the transition trace elements (TTE; Mn, Sc, Cr, V, Co, Ni, Cu, and Zn) range from 562 to 2395 ppm, 18.1 to 120.5 ppm, 29 to 74.1 ppm, 20.2 to 96.5 ppm, 25.5 to 91.7 ppm, 24.3 to 64.5 ppm, 10.76 to 45 ppm, and 37.9 to 78.4 ppm, respectively. Generally, the sandstones exhibit higher concentrations of the HFSEs and TTEs.

Averages of trace element concentrations of sandstones from the Elmina Sandstone Formation sandstones were normalized against the average Post-Archean Australian Shale (PAAS) data of Taylor and McLennan (1985), as shown in the spider diagram plot (Figure 12). Trace elements such as Zr, Hf, Y, Sc, and Co are highly enriched in the sandstones relative to PAAS. In contrast, depletion is observed in Rb, Sr, Nb, V, Cu, and Zn relative to PAAS. Overall, the sandstones are enriched in HFSEs and depleted in LILEs and TTEs relative to PAAS. The depletion of the LILEs (e.g Rb and Sr) in the sandstones is mainly controlled by the abundance of clay minerals. The observed depletion of Sr in the sandstone samples is likely related to feldspar weathering, as Sr is easily mobilized and adsorbed onto clay minerals.

Discussion

Petrography

In terms of petrography, the sandstones within the Ajua Shale and Elmina Sandstone Formations display distinctive textural characteristics. These include a very fine to fine-grained texture, a moderate to well-sorted arrangement, and subangular to subrounded shapes. These features collectively suggest a moderate transport distance and moderate reworking of the sandstones or sediments. Analyzing the data from the modal point counts for sandstones in both the Ajua Shale and Elmina Sandstone Formations (Table 3 and Table 4), it is evident that quartz constitutes the highest proportion of minerals, succeeded by feldspars and lithic fragments in order of decreasing abundance. The predominance of quartz grains over the other types of framework grains and high percentage of monocrystalline quartz over polycrystalline quartz grains in the sandstones from both Formations suggests a probable granitic and/or gneissic source (Tortosa et al., 1991). Also, the presence of heavy mineral inclusions in the quartz grains provides evidence of granitic sources (Morton, 1985; Morton and Johnsson, 1993). However, the occurrence of sedimentary and metamorphic lithics and strained polycrystalline quartz suggests minor contributions from probable sedimentary and metamorphic sources respectively.

Similar petrographic characteristics are observed in the other formations within the Sekondian Group, such as the Takoradi Sandstone and Essikado Sandstone Formation. These formations also show a predominance of quartz and feldspar, suggesting a common provenance from the Birimian terrane

Table 3. Petrographic Framework Composition and Modal Analysis (500-Point Counts) of Sandstone Samples from the Ajua Shale Formation

Sample ID	Quartz (Qz)					Feldspars (F)		Lithics (L)			Matrix	Accessory Minerals		
	Qm(non)	Qm(un)	Qp (2-3)	Qp (>3)	Q %	Pl	K	Ls	Lm	Lf %	Mx (%)	Ms	HM	Opq
AJ01	1	150	50	15	43.2	70	100	12	5	3.4	12.0	15	12	10
AJ03	2	140	45	10	39.4	80	110	13	5	3.6	14.0	10	10	5
AJ05	5	132	42	14	38.6	98	65	10	2	2.4	15.0	13	19	25
AJ06	5	145	47	12	41.8	87	106	7	1	1.6	15.4	6	6	1
AJ07	1	142	38	11	38.4	71	123	22	3	5.0	9.4	14	15	13
AJ08	1	162	55	11	45.8	55	115	21	2	4.6	10.0	10	11	7
AJ09	4	135	40	20	39.8	65	120	20	2	4.4	11.2	12	14	12
AS01	0	206	40	10	51.2	80	75	10	0	2.0	9.8	19	9	2
AS02	1	195	42	13	50.2	95	69	4	2	1.2	12.4	7	8	2
AS03	0	238	39	11	57.6	73	62	7	0	1.4	8.6	17	7	3
AS06	5	200	43	12	52.0	57	63	20	6	5.2	10.6	20	8	13
AS07	2	204	53	18	55.4	61	65	15	5	4.0	10.4	10	8	7
AS10	5	208	50	15	55.6	65	68	25	0	5.0	10.0	8	3	3
PU01	0	132	34	3	33.8	79	92	12	1	2.6	19.4	17	12	21
PU02	0	125	43	9	35.4	80	95	20	4	4.8	16.0	20	13	11
PU04	3	130	42	4	35.8	82	100	15	5	4.0	18.0	15	6	8
PU05	2	128	47	6	36.6	69	105	18	6	4.8	15.4	19	10	13
PU06	9	120	38	9	35.2	73	90	25	5	6.0	19.4	10	13	11
PU07	6	138	45	8	39.4	82	98	22	7	5.8	11.4	13	12	12
PU10	1	135	35	5	35.2	78	101	15	3	3.6	17.6	12	11	16

Qm(non) = Non-undulose Monocrystalline Quartz, Qm(un) = Undulose Monocrystalline, Quartz Qm = Monocrystalline quartz, Qp(2-3) = 2-3 Polycrystalline Quartz grains, Qp(>3) = > 3 Polycrystalline Quartz grains, Qp = Polycrystalline Quartz, Q = Quartz, Pl = Plagioclase, K = Alkali feldspar, F = Feldspar, Ls = Sedimentary Lithics, Lm= Metamorphic Lithics, Lv = Volcanic Lithics, Lf = Lithic Fragments, Mx = Matrix, Ms = Muscovite, HM = Heavy minerals, Opq = Opaques.

Table 3 Continued: Modal Analysis of Sandstone Samples in the Ajua Shale Formation in Volume Percentage (Vol %)

Sample ID	Qm	Qp	Pl	K	Ls	Lm	Q (total)	F (total)	L (total)	Lt (total)	Q %	F %	L %
AJ01	151	65	70	100	12	5	216	170	17	82	53.6	42.18	4.22
AJ03	142	55	80	110	13	5	197	190	18	73	48.64	46.91	4.44
AJ05	137	56	98	65	10	2	193	163	12	68	52.45	44.29	3.26
AJ06	150	59	87	106	7	1	209	193	8	67	50.98	47.07	1.95
AJ07	143	49	71	123	22	3	192	194	25	74	46.72	47.20	6.08
AJ08	163	66	55	115	21	2	229	170	23	89	54.27	40.28	5.45
AJ09	139	60	65	120	20	2	199	185	22	82	49.01	45.57	5.42
AS01	206	50	80	75	10	0	256	155	10	60	60.81	36.82	2.38
AS02	196	55	95	69	4	2	251	164	6	61	59.62	38.95	1.43
AS03	238	50	73	62	7	0	288	135	7	57	66.98	31.40	1.63
AS06	205	55	57	63	20	6	260	120	26	81	64.04	29.56	6.40
AS07	206	71	61	65	15	5	277	126	20	91	65.48	29.79	4.73
AS10	213	65	65	68	25	0	278	133	25	90	63.76	30.50	5.73
PU01	132	37	79	92	12	1	169	171	13	50	47.88	48.44	3.68
PU02	125	52	80	95	20	4	177	175	24	76	47.07	46.54	6.38
PU04	133	46	82	100	15	5	179	182	20	66	46.98	47.77	5.25
PU05	130	53	69	105	18	6	183	174	24	77	48.03	45.67	6.30
PU06	129	47	73	90	25	5	176	163	30	77	47.70	44.17	8.13
PU07	144	53	82	98	22	7	197	180	29	82	48.52	44.33	7.14
PU10	136	40	78	101	15	3	176	179	18	58	47.18	47.99	4.83

Qm = Monocrystalline quartz, Qp = Polycrystalline Quartz, Pl = Plagioclase, K = Alkali feldspar, Ls = Sedimentary Lithics, Lm = Metamorphic Lithics, Q = Quartz, F = Feldspar, L= Lithic Fragments, Lt = Total Lithics

Table 4. Petrographic Framework Composition and Modal Analysis (500-point counts) of Sandstone Samples from the Elmina Sandstone Formation

Sample ID	Quartz (Q)					Feldspars (F)		Lithics (L)			Matrix	Accessory Minerals			
	Qm(non)	Qm(un)	Qp(2-3)	Qp(>3)	Q %	Pl	K	Ls	Lm	Lf %	Mx (%)	Ms	Bt	HM	Opq
ECB01	3	105	42	23	34.6	65	90	30	1	6.2	20.0	18	10	5	8
ECB02	3	115	30	19	33.4	54	87	35	3	7.6	23.2	19	13	3	3
ECB02A	3	110	45	25	36.6	60	61	50	6	11.2	19.8	12	11	8	10
ECB03A	2	127	40	20	37.8	68	85	40	8	9.6	18.2	11	1	1	6
ECB04	0	125	47	15	37.4	50	74	48	10	11.6	17.4	20	12	7	5
ECB05	3	120	39	24	37.2	59	81	44	4	9.6	20.4	8	9	3	4
ECB06	4	180	76	25	57.0	47	7	44	5	9.8	15.8	17	3	4	9
ECB07	0	100	50	20	34.0	62	95	40	3	8.6	16.0	13	17	10	10
EG01	2	131	36	31	40.0	65	70	35	10	9.0	14.0	16	13	5	16
EG02	3	132	40	31	41.2	62	60	38	12	10.0	13.2	16	16	7	17
EG03	1	112	42	28	36.6	70	65	40	14	10.8	14.6	20	17	8	10
EG04	2	136	48	14	40.0	50	75	39	15	10.8	15.2	23	10	4	8
EG05	0	128	43	17	37.6	55	78	44	13	11.4	18.2	15	6	4	6
EG06	1	122	50	18	38.2	59	72	42	11	10.6	16.0	16	13	7	9
EG07	2	130	46	15	38.6	70	68	36	18	10.8	12.0	22	15	8	10
EL01	3	124	64	7	39.6	95	112	12	5	3.4	9.4	18	6	7	0
KD01	33	290	6	0	65.8	0	0	1	0	0.2	33.2	0	0	0	4
KD02	20	233	7	0	52.0	0	0	0	0	0.0	47.2	0	0	0	4
KD03	1	194	14	2	42.2	53	53	8	0	1.6	25.0	19	14	8	9
KD04	5	160	42	4	42.2	81	128	17	3	4.0	4.6	10	1	17	9

Qm(non) = Non-undulose Monocrystalline Quartz, Qm(un) = Undulose Monocrystalline, Quartz Qm = Monocrystalline quartz, Qp(2-3) = 2-3 Polycrystalline Quartz grains, Qp(>3) = > 3 Polycrystalline Quartz grains, Qp = Polycrystalline Quartz, Q = Quartz, Pl = Plagioclase, K = Alkali feldspar, F = Feldspar, Ls = Sedimentary Lithics, Lm= Metamorphic Lithics, Lv = Volcanic Lithics, Lf = Lithic Fragments, Mx = Matrix, Ms = Muscovite, Bt = Biotite, HM = Heavy minerals, Opq = Opaques.

Table 4 Continued: Modal Analysis of Sandstone Samples in the Elmina Sandstone Formation in Volume Percentage (Vol %)

Sample ID	Qm	Qp	Pl	K	Ls	Lm	Q (total)	F (total)	L (total)	Lt (total)	Q %	F %	L %
ECB01	108	65	65	90	30	1	173	155	31	96	48.19	43.18	8.64
ECB02	118	49	54	87	35	3	167	141	38	87	48.27	40.75	10.98
ECB02A	113	70	60	61	50	6	183	121	56	126	50.83	33.61	15.56
ECB03A	129	60	68	85	40	8	189	153	48	108	48.46	39.23	12.31
ECB04	125	62	50	74	48	10	187	124	58	120	50.68	33.60	15.72
ECB05	123	63	59	81	44	4	186	140	48	111	49.73	37.43	12.83
ECB06	184	101	47	7	44	5	285	54	49	150	73.45	13.92	12.63
ECB07	100	70	62	95	40	3	170	157	43	113	45.95	42.43	11.62
EG01	133	67	65	70	35	10	200	135	45	112	52.63	35.53	11.84
EG02	135	71	62	60	38	12	206	122	50	121	54.50	32.28	13.23
EG03	113	70	70	65	40	14	183	135	54	124	49.19	36.29	14.52
EG04	138	62	50	75	39	15	200	125	54	116	52.77	32.98	14.25
EG05	128	60	55	78	44	13	188	133	57	117	49.74	35.19	15.08
EG06	123	68	59	72	42	11	191	131	53	121	50.93	34.93	14.13
EG07	132	61	70	68	36	18	193	138	54	115	50.13	35.84	14.03
EL01	127	71	95	112	12	5	198	207	17	88	46.92	49.05	4.03
KD01	323	6	0	0	1	0	329	0	1	7	99.70	0.00	0.30
KD02	253	7	0	0	0	0	260	0	0	7	100.00	0.00	0.00
KD03	195	16	53	53	8	0	211	106	8	24	64.92	32.62	2.46
KD04	165	46	81	128	17	3	211	209	20	66	47.95	47.50	4.55

Qm = Monocrystalline quartz, Qp = Polycrystalline Quartz, Pl = Plagioclase, K = Alkali feldspar, Ls = Sedimentary Lithics, Lm= Metamorphic Lithics, Q = Quartz, F = Feldspar, L= Lithic Fragments, Lt = Total Lithics

and Pan-African mobile belt (Asiedu et al., 2005; Wilsona et al., 2022).

Sandstone Classification

The most widely used sandstone classification method is a combination of the matrix proportion (texture) with the percentage of framework grains (composition) (Baumann et al., 2016; Dickinson et al., 1983; Dott, 1964; Folk, 1980; Pettijohn et al., 1972). These sandstone classification schemes are based on the percentages of the framework grains (total quartz, feldspars and lithic fragments) in a Qt-F-L ternary diagram. In this study, the sandstones from the two Formations were classified based on classification schemes proposed by Pettijohn (1975) and Baumann et al. (2016). And also, the geochemical classification scheme after Herron (1988) was employed.

The sandstones of the Ajua Shale and Elmina Sandstone Formations have been classified mainly arkosic arenite with few sub-arkoses as seen in (Figure 2 and Figure 3). Feldspars constitute a range of approximately (24.0% to 38.8%, with an average of 33.22%) and (10.8% to 41.8%, with an average of 27.62%) of the overall framework grains found within the sandstones of both the Ajua Shale and Elmina Sandstone Formations respectively. The detrital framework grains within the analyzed sandstone samples are enclosed by a matrix, comprising approximately (8.6% to 19.4%, with an average of 13.3%) and (4.6% to 25.0%, with an average of 16.28%) of the overall rock composition of the Ajua Shale and Elmina Sandstone Formations respectively. Based on the percentages of the feldspar and matrix of the sandstones from both Formations (Table 3 and Table 4), they are both Arkosic and Sub-arkosic arenites as supported by the QFL ternary diagrams (Figure 2 and Figure 3).

However, there are some discrepancies comparing the petrographic and the geochemical classifications. The discrepancy between the geochemical and petrographic classification for the Ajua Shale sandstone samples could be as a result of the presence of lithic fragments alongside quartz and feldspar in the Ajua Shale sandstone samples which help justify the geochemical classification of some of the sandstones as litharenites. Also, it could be attributed to remnants of feldspar minerals were mistakenly identified as fresh feldspars during modal analysis. These remnants altered into clay, contributing to the high matrix content and causing the arkose to be classified as wackes. The Elmina sandstone samples geochemical classification as shales could be as a result of little or no pore spaces due to compaction and diagenesis altering their physical and chemical properties thereby making the rock exhibit characteristic more akin to shales. Also, the sublitharenites classification may be due to the presence of lithic fragments alongside quartz and feldspar minerals in the Elmina sandstones.

Sediment Maturity

Considering the modal mineralogy and sorting characteristics, studied sandstones from both the Ajua Shale and Elmina Sandstone Formations exhibit traits of being fine-grained, with sub-angular to sub-rounded grains, and demonstrating moderate to well sorting, implying a state of sub-maturity. These sandstones are primarily identified as arkosic arenite, with a smaller proportion being sub-arkosic arenite, indicating a slight degree of mineralogical maturity due to the presence of abundant quartz and fresh and slightly altered feldspar minerals. Ajua Shale and Elmina Sandstone Formation samples have ratio of $SiO_2/Al_2O_3 < 10$ with average values of (5.11 and 3.93) respectively suggesting chemical immaturity and reflects weak silicification and substantial aluminosilicate enrichment during diagenesis of the studies samples. The alkali content ($Na_2O + K_2O$), a measure of the feldspar content in the samples of the Ajua Shale Formation and Elmina Sandstone Formation with same average value of (6.28) respectively reflects the presence of feldspars suggesting low chemical maturity. Also, K_2O/Na_2O ratio < 1 with average values of (0.36 and 1.62) for the Ajua Shale Formation and Elmina Sandstone Formation samples similarly reported by Asiedu et al. (2005), indicates the predominance of the mineral plagioclase feldspar over mica and K-feldspar minerals, reflecting no to low K-metasomatism. Mineral dissolution and replacement during diagenesis are limited when there is no to low K-metasomatism resulting in low mineralogical maturity of the samples from both Formations.

Alternatively, Index of Compositional Variability (ICV) values of the Ajua Shale Formation sandstones and sandy shales and the Elmina Sandstone Formation sandstones are (average = 1.15, 1.26 and 1.25) respectively. The ICV typically registers its highest values in minerals that have experienced significant weathering, and it tends to decrease in minerals that are more stable and less weathered. Specifically, within clay minerals, the ICV decreases notably in the montmorillonite group and is at its lowest in the kaolinite group (Cox et al., 1995). Furthermore, shale that is more mature tends to exhibit low ICV values, usually below 1.0. In accordance with Cox et al. (1995), sandstones or shales with an ICV greater than 1.0 are considered compositionally immature, indicating that they originate from settings characterized by active tectonics during the deposition of the initial sediment cycle. Conversely, those with ICV values less than 1.0 are regarded as compositionally mature, signifying deposition in tectonically stable or cratonic environments where sediment recycling was less active. All the studied samples all have ICV values greater than 1 suggesting that the samples are compositionally immature and deposited in a tectonically active setting. The binary plot of CIA against ICV for the studied samples from both Formations (Figure 13) shows that most of the samples are geochemically immature and were derived from weakly weathered source rocks except for the very fine-grained sandstone sample from the Elmina Sandstone Formation that is matured and derived from intensively weathered source rock. According to Asiedu et al. (2005), other formations such as the Takoradi Sandstone and Essikado Sandstone within the Sekondian Group, also display similar sediment maturity char-

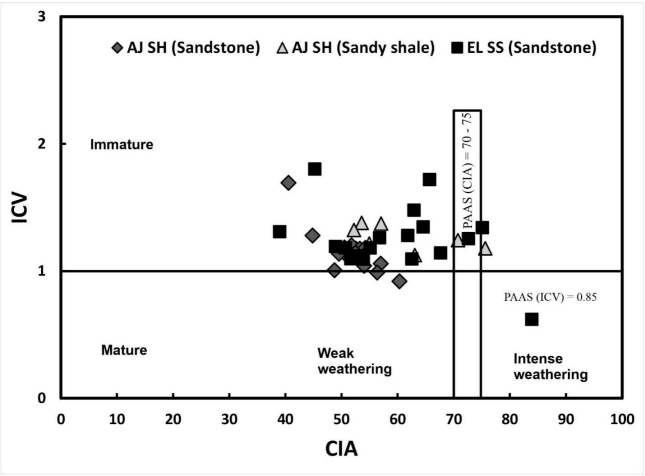

Figure 13. Binary plot of CIA against ICV for the Ajua Shale Formation samples; AJ SH (sandstones) and AJ SH (sandy shales) and Elmina Sandstone Formation samples; EL SS (sandstones).

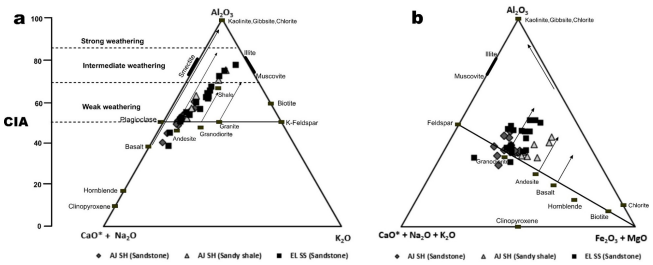

Figure 14. (a) A-CN-K and (b) A-CNK-FM plot (after Nesbitt and Wilson (1992); Nesbitt and Young (1984)) plots showing the weathering trend for the siliciclastic rocks of the Ajua Shale; AJ SH (Sandstones), AJ SH (Sandy shales) and Elmina Sandstone; EL SS (Sandstones) Formations

acteristics. The consistent presence of fresh feldspar and moderate sorting across these units suggests similar depositional environments and provenance.

Source Area Weathering and Paleoclimate

Condie (1993) assert that the characteristics of source rock, length of weathering process, climate, and rates of tectonic uplift in a source region all have significant impact on the chemical weathering of source rocks. Analyzing the interaction between Alkali and Alkaline Earth elements can help determine the degree and timing of weathering in siliciclastic deposits (Nesbitt and Young, 1982; Nesbitt and Wilson, 1992). According to Nesbitt and Young (1982, 1984); Nesbitt et al. (1996), Nesbitt and Wilson (1992), Taylor and McLennan (1985) and Fedo et al. (1995), the chemical weathering of feldspar minerals which make up about 75% of the earth's upper crust leads to the formation of secondary clay minerals. Chiefly, Ca, Na and K are eliminated from source rocks and the quantity of these elements that remain in sediments resulting from rocks serve as indicators of the intensity of chemical weathering. The weathering history of the sources of siliciclastic sediments can be deduced from the quantitative estimation of the chemical weathering of silicates such as the calculated values of Chemical Index of Alteration (CIA) by Nesbitt and Young (1982), Plagioclase Index of Alteration (PIA) by Fedo et al. (1995) and Chemical Index of Weathering (CIW) by Harnois (1988).

CIA values range from almost 50% for fresh rocks to 100% for completely weathered rocks. Consequently, CIA values increase with increasing weathering intensity, reaching the maximum 100%, which happens when all Ca, Na, and K have been removed from the weathering residue. The average CIA values of 51.82% and 61.03%for the sandstones and sandy shales of the Ajua Shale Formation, reflect relatively weak to intermediate degree of chemical weathering in the source area as shown in Figure 14(a). Also, CIA values of the Elmina Sandstone Formation sandstones (average = 59.46%) reflect relatively weak to intermediate degree of chemical weathering as seen in Figure 14(a). The low to intermediate CIA values of the samples from both Formation were also reported by Asiedu et al. (2005) with values ranging from (59% – 68%). CIW values of the Ajua Shale Formation sandstones and sandy shales (average = 55.65% and 67.63%) respectively reflect weak to intermediate chemical weathering. Also, CIW values of the Elmina Sandstone Formation sandstones (average = 66.50%) are reflective of weak to intermediate degree of chemical weathering.

In the A-CN-K diagram after Nesbitt and Young (1984) of the Ajua Shale Formation samples as seen in (Figure 14a), majority of the sandstones and all sandy shales plotted above the plagioclase and alkali feldspar line along the A-CN edge. This may be ascribed to the removal of Na and Ca from plagioclase at rates that are higher than the rates at which K is removed from microcline Nesbitt and Young (1984). The trend line when extended backward intersects the plagioclase-alkali feldspar line joining near the andesite field; a probable definitive source, close to the granodiorite. Also, in the ACNK-FM plot as shown in (Figure 14b) the sandy shales plot in the smectite and the sandstones plot towards the feldspar region following the projected weathering trend of andesite and granodiorite than mafic source rocks. Similarly, the A-CN-K diagram of the Elmina Sandstone Formation samples as shown in (Figure 14a), majority of the sandstones plotted above the plagioclase and alkali feldspar line along the A-CN edge. This also suggests the high removal rates of Na and Ca from plagioclase. The trend line of the sample plots follows the andesite and granodiorite lines with the possible ultimate source, close to the granodiorite. Also, in the ACNK-FM plot Figure 14(b), majority of the sandstones plot in the smectite and few towards the feldspar region following the predicted weathering trend of andesite and granodiorite than mafic source rocks.

Using the plagioclase index of alteration (PIA), source area weathering and elemental redistribution during diagenesis can also be evaluated. PIA measures the progressive weathering of feldspars to clay minerals (Fedo et al., 1995). Weathered plagioclase has a PIA value of 50%, while totally changed

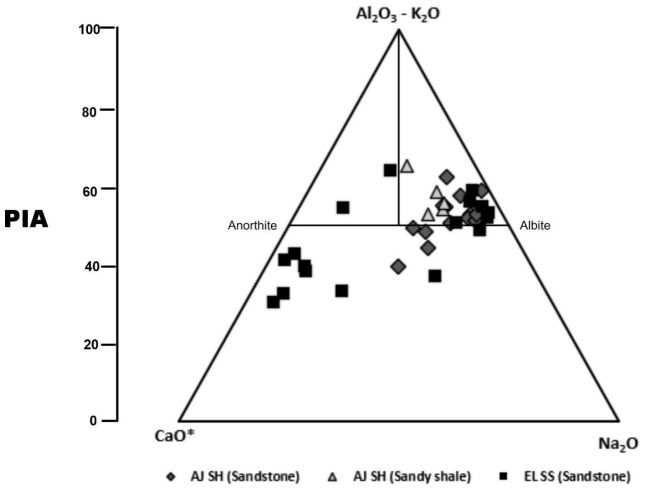

Figure 15. Ternary weathering diagram; AK-C-N (PIA) ternary plot (after (Fedo et al., 1995)) showing PIA- Ajua Shale Samples; AJ SH (Sandstone), AJ SH (Sandy Shale) and Elmina Sandstone samples; (EL SS (Sandstone)

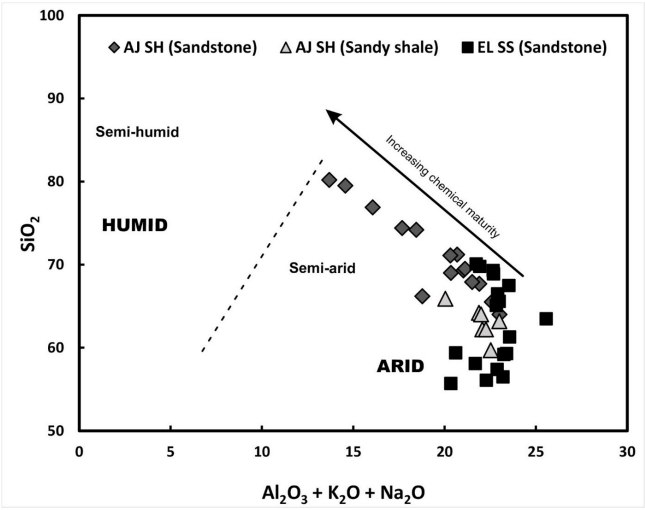

Figure 16. Paleoclimate and Chemical maturity (after Suttner et al. (1981)) of the Ajua Shale Formation samples; AJ SH (sandstones), AJ SH (sandy shales) and Elmina Sandstone Formation samples; EL SS (sandstones).

materials (such as kaolinite and gibbsite) have a maximum PIA value of 100%. PIA values of the Ajua Shale Formation sandstones and sandy shales (average = 52.26% and 64.24%) respectively reflect weak to intermediate chemical weathering of plagioclase minerals (Figure 15). Also, PIA values of the Elmina Sandstone Formation sandstones (average = 62.62%) reflect weak to intermediate degree chemical weathering of plagioclase minerals (Figure 15). These are evident in the petrographic studies where there is little or no sign of alteration of the plagioclase minerals observed in the studied samples.

Constraining the climatic condition during sedimentation of siliciclastic sedimentary rocks, the proposed plot by Suttner et al. (1981) was used to classify the maturity of Ajua Shale Formation (sandstones and sandy shales) and Elmina Sandstone Formation (sandstones) samples as a function of climate. Figure 16 shows that the sandstones and sandy shales of Ajua Shale Formation mostly plot in the field of arid to semi-arid climate respectively with increasing chemical maturity. Also, (Figure 16) shows all the sandstones of the Elmina Sandstone Formation plot in the arid climate field.

The paleoweathering indices of other Sekondian units, such as the Essikado Sandstone Formation, also reflect similar weathering intensities and paleoclimatic conditions. This consistency across the group supports a regional climatic influence during the Ordovician to Cretaceous periods (Asiedu et al., 2005).

Source Rock Composition

In terms of petrography, the sandstones within the Ajua Shale and Elmina Sandstone Formations display distinctive textural characteristics. These include a very fine to fine-grained texture, a moderate to well-sorted grains, and subangular to subrounded shapes. These features collectively suggest a moderate transport distance and moderate reworking of the sandstones. Analyzing the data from the modal point counts in both the Ajua Shale and Elmina Sandstone Formation sandstones as presented in Table 3 and Table 4 it is evident that quartz constitutes the highest proportion of minerals, succeeded by feldspars and lithic fragments in order of decreasing abundance. The predominance of quartz grains over the other types of framework grains and high percentage of monocrystalline quartz over polycrystalline quartz grains in the sandstones from both Formations suggests a probable granitic and/or gneissic source (Tortosa et al., 1991). Also, the presence of heavy mineral inclusions in the quartz grains provides evidence of granitic sources (Morton and Johnsson, 1993). However, the occurrence of sedimentary and metamorphic lithics and strained polycrystalline quartz suggests minor contributions from probable sedimentary and metamorphic sources respectively. The major elements and trace elements were also used to infer the provenance of the Ajua Shale and Elmina Sandstone Formations rocks.

The Al_2O_3 and TiO_2 ratio elements are commonly considered immobile during processes such as weathering, transportation, and diagenesis. Because of this, the ratio of Al_2O_3 to TiO_2 is frequently utilized to make inferences about the composition of the source rock (Absar and Sreenivas, 2015; Nagarajan et al., 2015; Zhao and Zheng, 2015). Hayashi et al. (1997) found that the Al_2O_3/TiO_2 ratio exhibits different ranges for various types of igneous rocks: 3 to 8 for mafic rocks, 8 to 21 for intermediate rocks, and 21 to 70 for felsic rocks. The Al_2O_3/TiO_2 ratio of the studied samples from the Ajua Shale (sandstones; average = 27.63, sandy shales; average = 21) and Elmina Sandstone Formations (sandstones; average = 29.10) indicates they were derived from a source dominated by felsic and intermediate igneous rocks (Figure 17(a)). There is an observed trend in TiO_2/Zr ratios that increases from felsic to mafic igneous source rocks, as described by Hayashi et al. (1997) and Wang et al. (2017). According to their findings, TiO_2/Zr ratios below 55 are indicative of felsic igneous rocks, ratios ranging from 55 to 200 suggest intermediate igneous

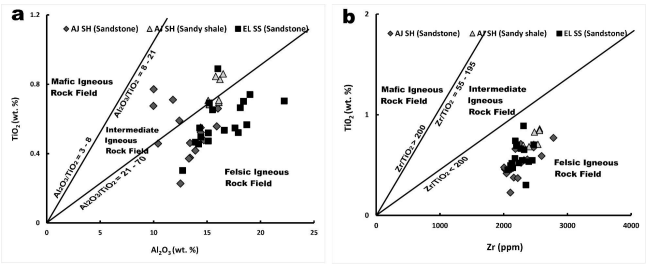

Figure 17. (a) TiO_2 – Al_2O_3 discrimination diagram (after (Hayashi et al., 1997)) showing AJ SH (Sandstones) and AJ SH (Sandy shales) from the Ajua Shale and EL SS (Sandstones) from the Elmina Sandstone Formations. (b) TiO_2 - Zr discrimination diagram after (Hayashi et al., 1997) showing; AJ SH (Sandstones), AJ SH (Sandy shales) from the Ajua Shale Formation and EL SS (Sandstones) from the Elmina Sandstone Formation.

rocks, and ratios exceeding 200 are associated with mafic igneous rocks. Furthermore TiO_2 - Zr discrimination diagram after Hayashi et al. (1997) for determining source area composition shows that the studied samples from both Ajua Shale and Elmina Sandstone Formations plot in the Felsic igneous rock field as shown in Figure 17(b) suggesting that the samples were derived from a felsic source area composition.

Zirconium (Zr), hafnium (Hf) and yittruim (Y) are considered indicators of source rock compositions due to their immobile characteristics (Taylor and McLennan, 1985). Moreover, these elements tend to selectively distribute into molten materials during the process of crystallization Feng and Kerrich (1990), leading to their higher concentration in felsic sources compared to mafic sources. The significant enrichment of the immobile trace elements Zr and Hf and slight enrichment of Y in the sandstones and shales of the Ajua Shale Formation (Sandstones: Zr average = 2262.13 ppm; Hf average = 19.23 ppm ; Y average = 22.38 ppm; Sandy shales: Zr average = 2474.57 ppm ; Hf average = 11.76; Y average = 34.9 ppm) and sandstones of Elmina Sandstone (Zr average = 2243 ppm; Hf average = 12.04 ppm ; Y average = 31.14 ppm) Formation as compared to UCC and PAAS (Figure 9 and Figure 12) is possibly linked to a felsic source rock composition.

The geochemical signatures of the other Sekondian units, such as the Takoradi Shale Formation and Effia Nkwanta Beds show enrichment in immobile trace elements like Zr and Hf, consistent with a felsic source (Asiedu et al., 2011, 2005).

Source Areas

The source rocks for the studied samples of the Ajua Shale and Elmina Sandstone Formations have been suggested to be of felsic and intermediate compositions, possible ultimate source of beingmainly granodiorites as highlighted by the A-CN-K and ACNK-FM diagrams of the Ajua Shale and Elmina Sandstone Formation samples (Figure 14). Notably, these granitoid rocks are found within the underlying Paleoproterozoic Birimian basement rocks of these two Formations. In Ghana, the Birimian terrane is made up of volcanic belts and sedimentary basins that have been affected by the intrusion of multiple generations of granitoids and have undergone metamorphism up to the amphibolite facies. The sedimentary basins are comprised of metamorphosed volcaniclastic rocks, wackes, and argillites Leube et al. (1990), while the volcanic belts are primarily composed of metamorphosed tholeiitic basaltic lavas containing volcaniclastics and calc-alkaline pyroclastics (Atta-Peters, 1996; Kesse, 1985)). According to Asiedu et al. (2005) based on geochemistry, Nd-Isotopes and model ages, the majority of Sekondian sedimentary rocks are believed to originate from the metasediments or granitoids present within the range of rock types in the Birimian terrane. However, there are exceptions like the Ajua Shale, Elmina Sandstones, and Essikado Sandstones Formations, which display minor contributions from detritus sourced from the Pan African Mobile Belt. The composition of these formations is a blend of detritus from the Birimian granitoids and/or felsic volcanic rocks, as well as felsic gneisses from the Pan-African mobile belt.

Tectonic Setting

Siliciclastic sedimentary rocks composition, major and trace element geochemistry are influenced by the makeup of their source rocks, which in turn are influenced by the tectonic setting. As a result, clastic sediments are likely to be classified based on the tectonic setting of their provenance (Bailey, 1981; Bhatia, 1983; Bhatia and Crook, 1986; McLennan et al., 1993; Roser and Korsch, 1986; Verma and Armstrong-Altrin, 2013, 2016).

Dickinson et al. (1983) stated that analyzing the QFL and QmFLt compositional diagrams can provide insights into the origin of sandstones as well as the tectonic environment in which they formed. In the case of the sandstones from the Ajua Shale and Elmina Sandstone Formations their positioning on the QFL diagram fall within the transitional continental and recycled orogenic fields as shown in Figure 18(a). However, the QmFLt diagram (Figure 18(b)) reveals most of the studied sandstones from the Ajua Shale and Elmina Sandstone Formations fall in the dissected arc fields. Siliciclastic rocks from various tectonic environments have geochemical traces that are unique to the terrain. For siliciclastic rocks that have not been significantly impacted by post-depositional weathering and metamorphism, tectonic setting discrimination diagrams produce credible results (McLennan et al., 1993). The major element based tectonic setting discrimination diagrams of Bhatia and Crook (1986) and Roser and Korsch (1986) are among the different tectonic setting discrimination diagrams that are frequently employed. Roser and Korsch (1986) categorized a series of tectonic plots in order to distinguish between the four basic tectonic settings of oceanic island arc (OIA), continental island arc (CIA), active continental margin (ACM), and passive continental margin. Based on the K_2O/Na_2O-SiO_2 discrimination diagram of Roser and Korsch (1986), all the Ajua Shale Formation and most of Elmina Sandstone Formations samples plot in the active continental field except two samples from the Elmina samples that plot one each in the passive and ocean island arc fields (Fig-

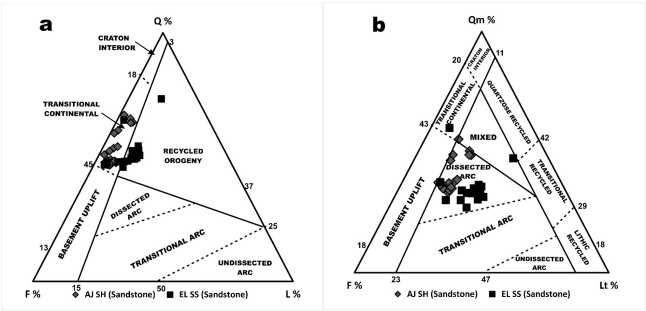

Figure 18. Tectono-provenance discrimination diagrams showing the relationship between framework composition of sandstones from the Ajua Shale; AJ SH (Sandstones) and Elmina Sandstone; EL SS (Sandstones) Formations and tectonic setting for determination of tectonic settings (after Dickinson et al. (1983))

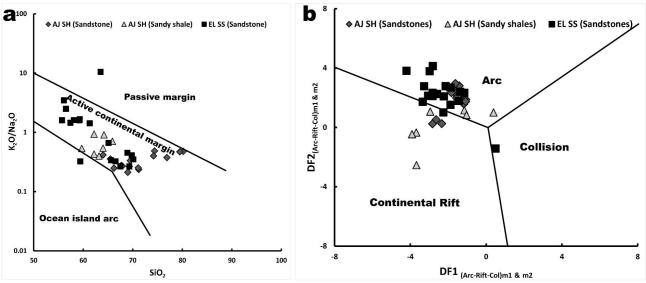

Figure 19. (a) K_2O/Na_2O vs. SiO_2 tectonic discrimination diagram (Roser and Korsch, 1986) for Siliciclastic rocks of the Ajua Shale; AJ SH (Sandstones), AJ SH (Sandy shales) and Elmina Sandstone; EL SS (Sandstones) Formations. (b) Discriminant-function multi-dimensional diagram for high silica clastic sediments (Verma and Armstrong-Altrin, 2013) showing the tectonic setting for the Ajua Shale; AJ SH (Sandstones), AJ SH (Sandy shales) and El mina Sandstone; EL SS (Sandstones) Formations.

ure 19(a)). Similarly, using the relevant discriminant-function multi-dimensional diagram of (Verma and Armstrong-Altrin, 2013) for high-silica and low silica clastic sediments shows that most of the samples from the Ajua Shale and Elmina Sandstone Formations are deposited in the arc and a few in the continental rift setting (Figure 19(b)).

Further differentiation of the tectonic setting of the Ajua Shale and Elmina Sandstone Formations was conducted using the new discriminant diagrams suggested by Verma and Armstrong-Altrin (2016). All the studied samples from both formations fall in the active margin field (Figure 20).

According to Gao and Wedepohl (1995) and Cullers and Podkovyrov (2000) CIA and ICV values can be used to deduce tectonic settings. Sedimentary rocks characterized by a combination of low CIA and high ICV values, specifically when CIA is less than 60 and ICV is greater than 1, are typically sourced from active arc settings. Conversely, sedimentary rocks with high CIA and low ICV values, typically when CIA exceeds 75 and ICV is less than 1, are usually derived from passive margins. The studied samples from the Ajua Shale and Elmina Sandstone Formations have CIA values below

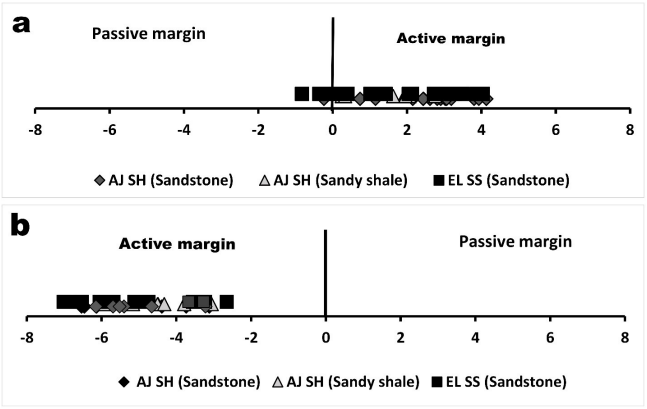

Figure 20. Tectonic setting discrimination diagram based on major oxides and major oxides and trace elements for the Ajua Shale; AJ SH (Sandstones, AJ SH (Sandy shales) and Elmina Sandstone; EL SS (Sandstones) Formations (after Verma and Armstrong-Altrin (2016)); (a) based on major oxides DF(A-P)M and (b) based on major oxides and trace element DF(A-P)MT

60 and ICV values above 1 suggesting an active arc tectonic setting which is consistent with interpretation derived from the discrimination diagrams. This interpretation aligns with previous studies by Asiedu et al. (2011, 2005) that inferred active tectonic setting for samples from the Ajua Shale and Elmina Sandstone Formations. Other formations within the Sekondian Group, such as the Takoradi Shale Formation and Effia Nkwanta Beds, also indicate deposition in active tectonic settings. The presence of similar geochemical signatures and tectonic discrimination results across these units reinforces the interpretation of an active margin setting for the Sekondian Group (Asiedu et al., 2011, 2005).

However, there are certain factors that challenge the inference that these sediments were deposited in an active tectonic setting. One key point is the absence of Ordovician igneous rocks and absence of volcanic lithics in the sandstones. Also, the low sedimentation rate and short thickness (1200 m). The Sekondian Group is about 1200m thick. The oldest formation, i.e., Ajua Shale is late Ordovician in age, and the youngest formation, i.e., the Essikado Sandstone is early Cretaceous, suggesting that the duration of deposition of the Sekondian Group is about 300 m.y. The rate of deposition of the Sekondian may therefore be estimated at about 4 meters/million years (1200 m/300 m.y.). This apparent low sedimentation rate of the entire Sekondian Group suggest deposition in passive margin setting. The lack of such features raises doubts about the samples being deposited in an active margin. Additionally, the absence of direct field evidence of tectonic uplifts in southern Ghana during the early Paleozoic era further questions the interpretation of an active margin. The observed faults in the study area are of Jurassic age Crow (1952), suggesting a different tectonic event associated with the rift between South America and the African continent in the Aptian to Albian times (Asiedu et al., 2011, 2005).

In summary, the petrographic and geochemical signatures

observed in the Ajua Shale and Elmina Sandstone Formations samples, such as immature sediments (high ICV values), the moderate occurrence of unstable minerals such as plagioclase, low weathering indices (i.e., CIA, PIA values) and plots on various tectonic discrimination diagrams (i.e., Figure 18, Figure 19, Figure 20) suggest high sedimentation rate and, therefore, active tectonic setting. Overall, the Ordovician period (age of the Ajua Shale and Elmina Sandstone Formations) is characterized by extensive global tectonic events and volcanic activity, significant shifts in plate tectonics and geographic arrangements, and the presence of vast oceans that separated numerous major landmasses (Cocks and Torsvik, 2021). However, in very cold and arid climates areas, the intensity of chemical weathering may be low, even when sedimentation rates are low. Therefore, it is possible for passive (inactive) setting sediments in cold/arid climates to show petrographic and geochemical signatures observed in the Ajua Shale and Elmina Sandstone Formations. The Ajua Shale and Elmina Sandstone Formations were affected by the Late Ordovician glaciation, and paleomagnetic data show that the formations were located in high southerly paleolatitudes, with North Africa situated on the south magnetic pole (Asiedu et al., 2011). Field evidence of glacial conditions for the Ajua Shale Formation includes the occurrence of diamictites, glacial varves, and dropstones.

Conclusion

A unified method of petrography, mineralogy and geochemistry was used to infer the provenance of both the Ajua Shale and Elmina Sandstone Formations as follows;

- The (QFL) provenance discriminant diagram reveals mainly a recycled and a transitional source nature of the studied samples from the Ajua Shale and Elmina Sandstone Formations respectively. Also, the (QmFLt) provenance discriminant diagram reveals a dissected arc source nature of the studied sandstone samples from both Formations. All these sources are consistent with the sediments from the Birimian.
- Geochemically, the paleo weathering intensity and paleoclimate of the studied samples of the Ajua Shale and Elmina Sandstone Formations deduced from CIA, CIW, PIA, ICV and CIA verses ICV plots reveal a weak to moderate chemical weathering, chemically immature sediments and a paleoclimatic condition of semi-arid to arid.
- The provenance based on multiple geochemical discriminant diagrams reveals felsic to intermediate source rock characteristics and an inferred source from a mixture of detritus from the Birimian granitoids and/or felsic gneisses of the Pan African mobile belt deposited in an active margin setting. However, the absence of volcanic features and the lack of direct evidence for tectonic uplifts challenge the active margin tectonic setting interpretation. Instead, the presence of granitoids with juvenile arc setting signatures supports the idea.

References

Absar, N. and Sreenivas, B. (2015). Petrology and geochemistry of greywackes of the 1.6 ga middle aravalli supergroup, northwest india: evidence for active margin processes. *International Geology Review*, 57(2):134–158.

Anan-Yorke, R. (1974). Devonian chitinozoans and acritarcha from exploratory oil wells on the shelf and coastal regions of ghana, west africa. *Ghana Geol. Surv. Bull.*, 37:217.

Anani, C. Y., Kwayisi, D., Agra, N. A., and Asiedu, D. K. (2018). Provenance of shales and sandstones from the devonian accraian group, southern ghana. *Geosciences Journal*, 22(3).

Armstrong-Altrin, J. S., Lee, Y. I., Kasper-Zubillaga, J. J., and Trejo-Ramírez, E. (2017). Mineralogy and geochemistry of sands along the manzanillo and el carrizal beach areas, southern mexico: implications for palaeoweathering, provenance and tectonic setting. *Geological Journal*, 52(4):559–582.

Armstrong-Altrin, J. S., Nagarajan, R., Balaram, V., and Natalhy-Pineda, O. (2015). Petrography and geochemistry of sands from the chachalacas and veracruz beach areas, western gulf of mexico, mexico: constraints on provenance and tectonic setting. *Journal of South American Earth Sciences*, 64:199–216.

Armstrong-Altrin, J. S., Nagarajan, R., Lee, Y. I., Zubillaga, J. J. K., and Saldaña, L. P. C. (2014). Geochemistry of sands along the san nicolás and san carlos beaches, gulf of california, mexico: implications for provenance and tectonic setting. *Turkish Journal of Earth Sciences*, 23(5):533–558.

Armstrong-Altrin, J. S., Nagarajan, R., Madhavaraju, J., Rosalez-Hoz, L., Lee, Y. I., Balaram, V., and Avila-Ramírez, G. (2013). Geochemistry of the jurassic and upper cretaceous shales from the molango region, hidalgo, eastern mexico: Implications for source-area weathering, provenance, and tectonic setting. *Comptes Rendus Geoscience*, 345(4):185–202.

Asiedu, D. K., Atta-Peters, D., Hegner, E., Rocholl, A., and Shibata, T. (2011). Palaeoclimatic control on the composition of palaeozoic shales from southern ghana, west africa. *Ghana Mining Journal*, 12:7–16.

Asiedu, D. K., Atta-Peters, D., and Peprah, R. (2000). Depositional environment of the takoradi sandstone formation of the sekondian group, western ghana, as revealed by textural analysis. *Ghana Min. J.*, 6:53–58.

Asiedu, D. K., Hegner, E., Rocholl, A., and Atta-Peters, D. (2005). Provenance of late ordovician to early cretaceous sedimentary rocks from southern ghana, as inferred from nd isotopes and trace elements. *Journal of Africa Earth Sciences*.

Atta-Peters, D. (1996). Latest devonian and early carboniferous miospores from the takoradi shale formation of the sekondian group, western ghana. *Afr. Geosci. Rev.*, 3:413–427.

Atta-Peters, D. (1999). Upper devonian acritarchs from the lower takoradi shales of the sekondian group. *Ghana Min. J.*, 5:1–10.

Atta-Peters, D. (2000). Early cretaceous miospores from the essikado sandstone formation of the sekondian group of ghana. *Rev. Esp. Micropaleontol.*, 32:245–257.

Bailey, J. C. (1981). Geochemical criteria for a refined tectonic discrimination of orogenic andesites. *Chemical Geology*, 32(1–4):139–154.

Baumann, S. D., Cory, A. B., and Dylka, S. K. (2016). Lithostratigraphic interpretation and redefinition of the sedimentary clastic assemblage (bayfield group, and jacobsville sandstone) in michigan and wisconsin, usa and ontario, canada. *Stratigraphy*, 13(3):163–181.

Bhatia, M. R. (1983). Plate tectonics and geochemical composition of sandstones. *The Journal of geology*, 91(6):611–627.

Bhatia, M. R. and Crook, K. A. (1986). Trace element characteristics of graywackes and tectonic setting discrimination of sedimentary basins. *Contributions to mineralogy and petrology*, 92(2):181–193.

Cocks, L. R. M. and Torsvik, T. H. (2021). Ordovician palaeogeography and climate change. *Gondwana Research*, 100:53–72.

Condie, K. C. (1993). Chemical composition and evolution of the upper continental crust: contrasting results from surface samples and shales. *Chemical geology*, 104(1–4):1–37.

Cox, R., Lowe, D. R., and Cullers, R. L. (1995). The influence of sediment recycling and basement composition on evolution of mudrock chemistry in the southwestern united states. *Geochimica et Cosmochimica Acta*, 59(14):2919–2940.

Crow, A. T. (1952). *The rocks of the Sekondi Series of the Gold Coast*. Gold Coast Geological Survey Bulletin No. 18, William Lewis Ltd.

Cullers, R. L. and Podkovyrov, V. N. (2000). Geochemistry of the mesoproterozoic lakhanda shales in southeastern yakutia, russia: implications for mineralogical and provenance control, and recycling. *Precambrian Research*, 104(1–2):77–93.

Dickinson, W. R. (1970). Interpreting detrital modes of greywacke and arkose. *J. Sediment. Petrol.*, 40:695–707.

Dickinson, W. R., Beard, L. S., Brakenridge, G. R., Erjavec, J. L., Ferguson, R. C., Inman, K. F., and Ryberg, P. T. (1983). Provenance of north american phanerozoic sandstones in relation to tectonic setting. *Geological Society of America Bulletin*, 94(2):222–235.

Dott, R. H. (1964). Wacke, graywacke and matrix; what approach to immature sandstone classification? *Journal of Sedimentary Research*, 34(3):625–632.

Fedo, C. M., Wayne Nesbitt, H., and Young, G. M. (1995). Unraveling the effects of potassium metasomatism in sedimentary rocks and paleosols, with implications for paleoweathering conditions and provenance. *Geology*, 23(10):921–924.

Feng, R. and Kerrich, R. (1990). Geochemistry of fine-grained clastic sediments in the archean abitibi greenstone belt, canada: implications for provenance and tectonic setting. *Geochimica et Cosmochimica Acta*, 54(4):1061–1081.

Folk, R. L. (1980). *Petrology of sedimentary rocks*. Hemphill publishing company.

Gao, S. and Wedepohl, K. H. (1995). The negative eu anomaly in archean sedimentary rocks: Implications for decomposition, age and importance of their granitic sources. *Earth and Planetary Science Letters*, 133(1–2):81–94.

Harnois, L. (1988). The ciw index: a new chemical index of weathering. *Sedimentary Geology*, 55(3):319–322.

Hayashi, K. I., Fujisawa, H., Holland, H. D., and Ohmoto, H. (1997). Geochemistry of 1.9 ga sedimentary rocks from northeastern labrador, canada. *Geochimica et Cosmochimica Acta*, 61(19):4115–4137.

Herron, M. M. (1988). Geochemical, classification of terrigenous sands and shales from core or log data. *Journal of Sedimentary Research*, 58(5):820–829.

Kesse, G. O. (1985). The mineral and rock resources of ghana.

Leube, A., Hirdes, W., Mauer, R., and Kesse, G. O. (1990). The early proterozoic birimian supergroup of ghana and some aspects of its associated gold mineralization. *Precambrian research*, 46(1–2):139–165.

McLennan, S. M., Hemming, S., McDaniel, D. K., and Hanson, G. N. (1993). Geochemical approaches to sedimentation, provenance, and tectonics. *Special Papers-Geological Society of America*, pages 21–25.

McLennan, S. M., Taylor, S. R., McCulloch, M. T., and Maynard, J. B. (1990). Geochemical and nd sr isotopic composition of deep-sea turbidites: crustal evolution and plate tectonic associations. *Geochimica et cosmochimica acta*, 54(7):2015–2050.

Mensah, M. (1973). On the question of the age of the sekondi series, upper devonian or lower carboniferous rocks of ghana. *Ghana J. Sci.*, 13:134–139.

Morton, A. C. (1985). Heavy minerals in provenance studies. In *Provenance of arenites*, pages 249–277. Springer Netherlands.

Morton, A. C. and Johnsson, M. J. (1993). Factors influencing the composition of detrital heavy mineral suites in holocene sands of the apure river drainage basin, venezuela.

Nagarajan, R., Armstrong-Altrin, J. S., Kessler, F. L., Hidalgo-Moral, E. L., Dodge-Wan, D., and Taib, N. I. (2015). Provenance and tectonic setting of miocene siliciclastic sediments, sibuti formation, northwestern borneo. *Arabian Journal of Geosciences*, 8:8549–8565.

Nagarajan, R., Franz L, K., Jong, J., Muthuvairavasamy, R., Muhammad, A. A., Dayong, V., and Kinanthi, D. (2021). Geochemistry of the palaeocene-eocene upper kelalan formation, nw borneo: Implications on palaeoweathering, tectonic setting, and provenance. *Geological Journal*, 56(5):2500–2527.

Nesbitt, H. and Young, G. M. (1982). Early proterozoic climates and plate motions inferred from major element chemistry of lutites. *nature*, 299(5885):715–717.

Nesbitt, H. W. and Wilson, R. E. (1992). Recent chemical weathering of basalts. *American Journal of science*, 292(10):740–777.

Nesbitt, H. W. and Young, G. M. (1984). Prediction of some weathering trends of plutonic and volcanic rocks based on thermodynamic and kinetic considerations. *Geochimica et cosmochimica acta*, 48(7):1523–1534.

Nesbitt, H. W., Young, G. M., McLennan, S. M., and Keays, R. R. (1996). Effects of chemical weathering and sorting on the petrogenesis of siliciclastic sediments, with implications for provenance studies. *The Journal of Geology*, 104(5):525–542.

Osae, S., Asiedu, D. K., Banoeng-Yakubo, B., Koeberl, C., and Dampare, S. B. (2006). Provenance and tectonic setting of late proterozoic buem sandstones of southeastern ghana: Evidence from geochemistry and detrital modes. *Journal of African Earth Sciences*, 44(1):85–96.

Pettijohn, F. J. (1975). *Sedimentary rocks*, volume 3. Harper & Row.

Pettijohn, F. J., Potter, P. E., and Siever, R. (1972). Petrographic classification and glossary.

Roser, B. P. and Korsch, R. J. (1986). Determination of tectonic setting of sandstone-mudstone suites using sio2 content and k2o/na2o ratio. *The Journal of Geology*, 94(5):635–650.

Suttner, L. J., Basu, A., and Mack, G. H. (1981). Climate and the origin of quartz arenites. *Journal of Sedimentary Research*, 51(4):1235–1246.

Taylor, S. R. and McLennan, S. M. (1985). The continental crust: its composition and evolution.

Tortosa, A., Palomares, M., and Arribas, J. (1991). Quartz grain types in holocene deposits from the spanish central system: some problems in provenance analysis. *Geological Society, London, Special Publications*, 57(1):47–54.

Verma, S. P. and Armstrong-Altrin, J. S. (2013). New multidimensional diagrams for tectonic discrimination of siliciclastic sediments and their application to precambrian basins. *Chemical Geology*, 355:117–133.

Verma, S. P. and Armstrong-Altrin, J. S. (2016). Geochemical discrimination of siliciclastic sediments from active and passive margin settings. *Sedimentary Geology*, 332:1–12.

Wang, Z., Wang, J., Fu, X., Zhan, W., Yu, F., Feng, X., and Zeng, S. (2017). Organic material accumulation of carnian mudstones in the north qiangtang depression, eastern tethys: controlled by the paleoclimate, paleoenvironment, and provenance. *Marine and Petroleum Geology*, 88:440–457.

Wilsona, M. C., Asumahb, T. A., Emmahamb, J. T., and Asanteb, K. K. (2022). Comparative studies of some of the rocks in the sekondian series–implications for petromechanical strength of the rocks. *Earth Sciences Malaysia (ESMY)*, 6(1):32–39.

Zhao, M. Y. and Zheng, Y. F. (2015). The intensity of chemical weathering: Geochemical constraints from marine detrital sediments of triassic age in south china. *Chemical geology*, 391:111–122.